THE PENNSYLVANIA
STATE UNIVERSITY

IONOSPHERIC RESEARCH

Scientific Report No. 326

MOLECULAR FLOW THROUGH MEMBRANES

by
R. E. Pulfrey
November 10, 1968

IONOSPHERE RESEARCH LABORATORY

University Park, Pennsylvania NASA Grant NGR 39-009-032

Ionospheric Research

NASA Grant NGR 39-009-032

Scientific Report

on

"Molecular Flow Through Membranes"

by

R. E. Pulfrey

November 10, 1968

Scientific Report No. 326

Ionosphere Research Laboratory

Submitted by: B. R. F. Kendall (au)

B. R. F. Kendall, Associate Professor of Physics

Approved by: A. H. Waynick

A. H. Waynick, Professor of Electrical Engineering,
Director, Ionosphere Research Laboratory

The Pennsylvania State University

College of Engineering

Department of Electrical Engineering

TABLE OF CONTENTS

ABSTRACT

The objects of the following work are these:

a. To show how the theory of molecular flow can be used for analysis of vacuum networks;

b. To determine experimentally the highest pressures for which molecular flow is maintained through a membrane (two different types tested) for various isotopically pure gases;

c. To show the results of experiments with a simple molecular flow network;

d. To point out that the experimental method presented herein constitutes an extremely accurate method for measuring the absolute conductance of a membrane for molecular gas flow;

e. To show how to optimize a vacuum network for analysis of a gas mixture by the variation in effusion rates of the constituents of the mixture;

f. To discuss some advantages, limitations and the expected accuracy of such a method of gas mixture analysis;

g. To show numerical methods of increasing the accuracy of this method of gas mixture analysis.

CHAPTER I

INTRODUCTION

1.1 Definition of Molecular Flow

If a gas is flowing in a system at a pressure sufficiently low so that the mean free path is long compared to the diameter of the flow tube, then there will be relatively few intermolecular collisions compared to the number of collisions with the walls, and molecular flow is said to be taking place.

The approximate condition usually given for molecular flow is that the Knudsen number

$$n \equiv L/d > 1$$

where L is the mean free path of the gas and d is a characteristic dimension, usually diameter, of the flow channel.

1.2 Previous Investigations of Molecular Flow

The early work on molecular flow was done by Knudsen (1909) and (1911), Smoluchowski (1910) and Gaede (1913). These investigations were extended by Adzumi (1937), and a great deal of work was done by Clausing (1929) and (1932) on molecular flow in tubes of various lengths.

More recent studies have detailed interesting molecular flow effects in both long and short tubes, and at the transition between molecular and slip flow. The results of Clausing have been extended by Pollard and Present (1948), Iczkowski, et al, (1963) and Barrer and Nicholson (1965) and (1966).

Molecular flow through long pores has been discussed by Wheeler (1951), Carman (1956), Scheidegger (1960) and Hirsch (1961). The transition between molecular and slip flows has been analyzed by Pollard and Present (1948), Scott and Dullien (1962) and Fryer (1966).

The effusion of gas through a small hole was used by Buckingham and Edwards (1920) for a rough determination of gas densities. Eden (1951) suggested that an approximation to the pressure vs time curve of a gas mixture could be used to obtain an average molecular weight. Kendall (1966) pointed out the possibility of obtaining the composition of a gas mixture from its pressure vs time curve for molecular effusion through small holes.

1.3 Possibility of Using Molecular Flow to Analyze a Gas Mixture

If there is molecular flow at constant temperature, it is easily shown from simple kinetic theory that effusion of an isotopically pure gas through a single thin membrane from one chamber to another at a lower initial pressure takes place according to the law

$$P(t) = P_o\, e^{-\lambda t} .$$

where P_o and $P(t)$ are the initial and time dependent pressure differences across the membrane and λ is a constant dependent upon the particular geometry and species of gas.

For N different species of gas present and effusing independently this equation becomes

$$P(t) = P_o \sum_{j=1}^{N} X_j\, e^{-\lambda_j t}, \qquad (1)$$

with

$$\sum_{j=1}^{N} X_j = 1$$

where X_j is the mole fraction of the j^{th} species present.

If the pressure $P(t_i)$ is measured at N points in time t_i then Equation (1) becomes the system

$$P(t_i) = P_o \sum_{j=1}^{N} X_j \, e^{-\lambda_j t_i} \qquad (2)$$

where i = 1, 2, ... N is the index on the data points and N is the number of gases in the mixture. If the λ_j have been determined, the linear system (2) may be solved for the X_j as unknowns. Thus, in principle, a membrane and a pressure gauge can be used as a mass spectrometer to analyze a mixture of gases (Kendall, 1966).

CHAPTER II

THEORY OF A MOLECULAR EFFUSION GAS ANALYZER

2.1 Vacuum-Electrical Analogy

The mathematical analogies between an electric circuit and a vacuum system having molecular flow have been used for vacuum system calculations by Dushman (1962), Teubner (1962), Barnes (1964), Kendall (1968) and Kendall and Pulfrey (1969).

Consider a gas flowing in a channel under conditions of molecular flow between a variable volume V_1 at pressure P_1 and temperature T and a second variable volume V_2 at pressure P_2 and at the same temperature T. The standard definition (Dushman, 1962) for flow rate Q leaving volume V_1 is

$$-Q \equiv P_1 \frac{\partial V_1}{\partial t}\Bigg)_{P_1} .$$

If there is molecular flow the ideal gas law may be assumed to hold, and at constant P_1, P_2, T we have

$$-Q \equiv P_1 \frac{\partial V_1}{\partial t}\Bigg)_{P_1} = kT \frac{\partial N_1}{\partial t}$$

$$= - P_2 \frac{\partial V_2}{\partial t}\Bigg)_{P_2} = - kT \frac{\partial N_2}{\partial t}$$

where k is Boltzman's constant and N_1 and N_2 are the numbers of molecules in volumes V_1 and V_2, and t is time.

The conductance F_{12} of the channel connecting V_1 and V_2 is defined from the equation

$$Q\left[-\left(\frac{\partial V_1}{\partial t}\right)_{P_1}^{-1} - \left(\frac{\partial V_2}{\partial t}\right)_{P_2}^{-1}\right] = P_1 - P_2 \equiv Q/F_{12}.$$

From this definition the analogy with Ohm's law may immediately be seen where

$$Q \longleftrightarrow \text{current}$$

$$P_1 - P_2 \longleftrightarrow \text{potential difference}$$

$$F_{12} \longleftrightarrow \text{electrical conductance.}$$

It is clear that the conductance F_{12} depends directly upon the molecular velocity and, hence, inversely upon the square root of the molecular weight (for molecular flow at a particular temperature).

Also

$$F_{12} = F_{21}.$$

Comparison of the equation for a variable capacitance c having a constant voltage v maintained across it

$$i = v\left(\frac{\partial c}{\partial t}\right)_v$$

where i is the current leaving the capacitance, with the definition

$$-Q \equiv P\left(\frac{\partial V}{\partial t}\right)_P$$

leads to the analogy

$$\text{volume} \longleftrightarrow \text{capacitance.}$$

2.2 Analysis of a Simple Vacuum System

As an example of this approach to analyzing vacuum systems

having molecular flow, consider the system of Figure 1. In this system the membrane M can be moved impulsively from position A to position B creating an instantaneous pressure difference, and if the membrane holes are small enough, there will be molecular flow through the membrane M.

The pressure response of this system with molecular flow will be found by analogy with the circuit of Figure 2a using initial conditions on the charges

$$q_1(0) = q_2(0) = q_0$$

and also defining the current i

$$i = -\frac{dq_1}{dt} = \frac{dq_2}{dt} .$$

At time t = 0 the capacitances are changed by an amount Δ as shown, and for t > 0 the loop equation is

$$\frac{q_1}{C + \Delta} - iR - \frac{q_2}{C - \Delta} = 0.$$

Using the definition of i above and the fact that

$$q_1(t) + q_2(t) = 2q_0$$

then

$$-\frac{q_2 - 2q_0}{C + \Delta} - R\frac{dq_2}{dt} - \frac{q_2}{C - \Delta} = 0,$$

$$\frac{dq_2}{dt} + \frac{1}{R}\left(\frac{C - \Delta + C + \Delta}{C^2 - \Delta^2}\right) q_2 - \frac{2q_0}{R(C + \Delta)} = 0.$$

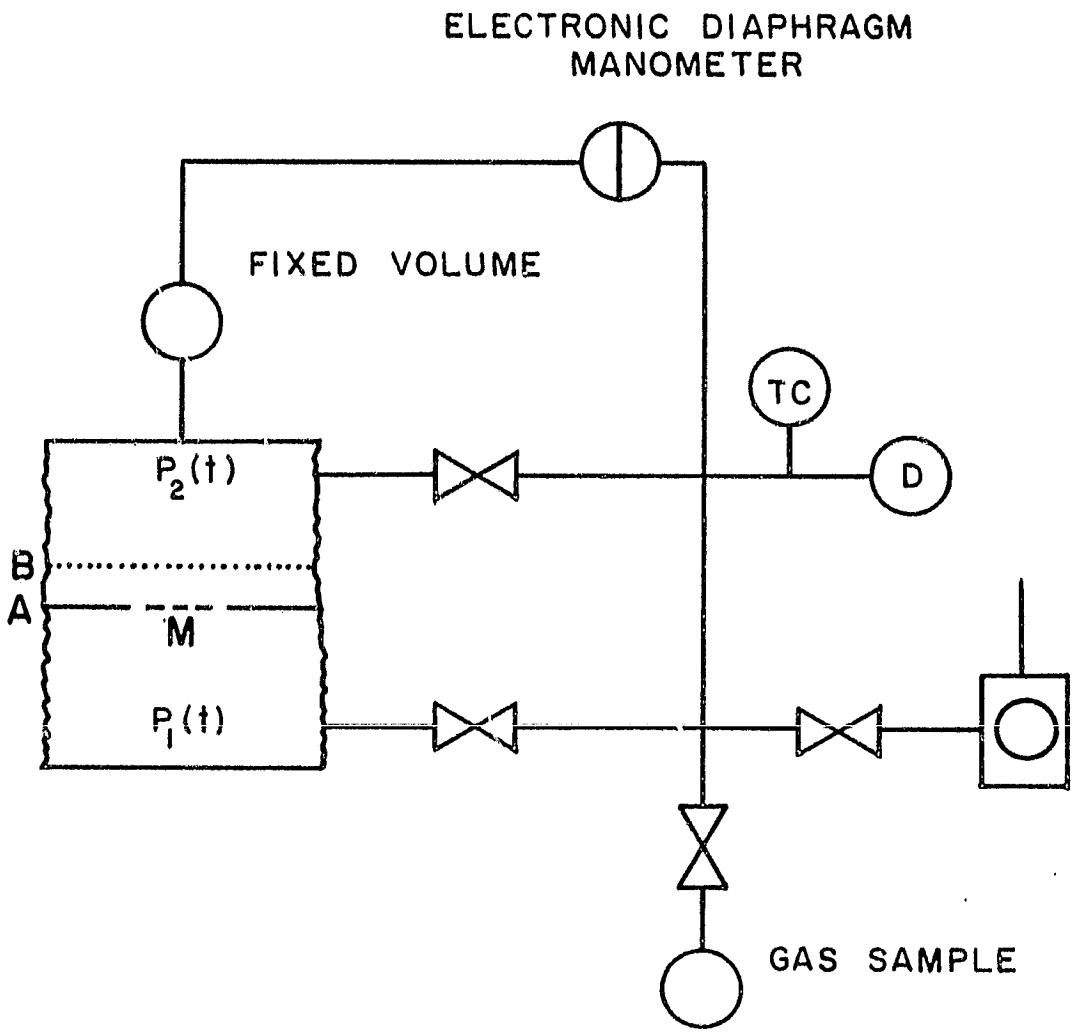

FIGURE 1 VACUUM SYSTEM WITH SINGLE MEMBRANE

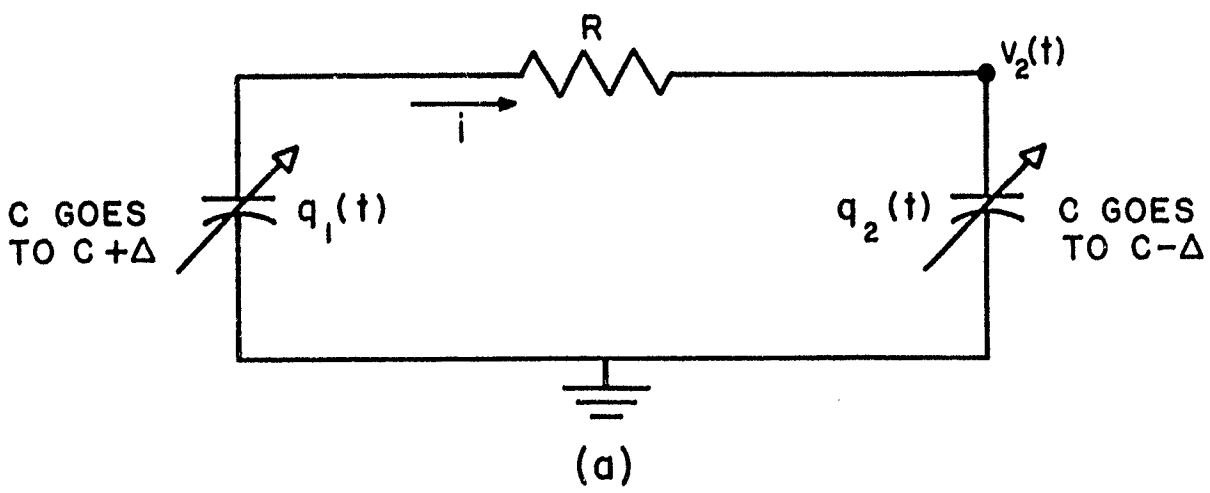

(a)

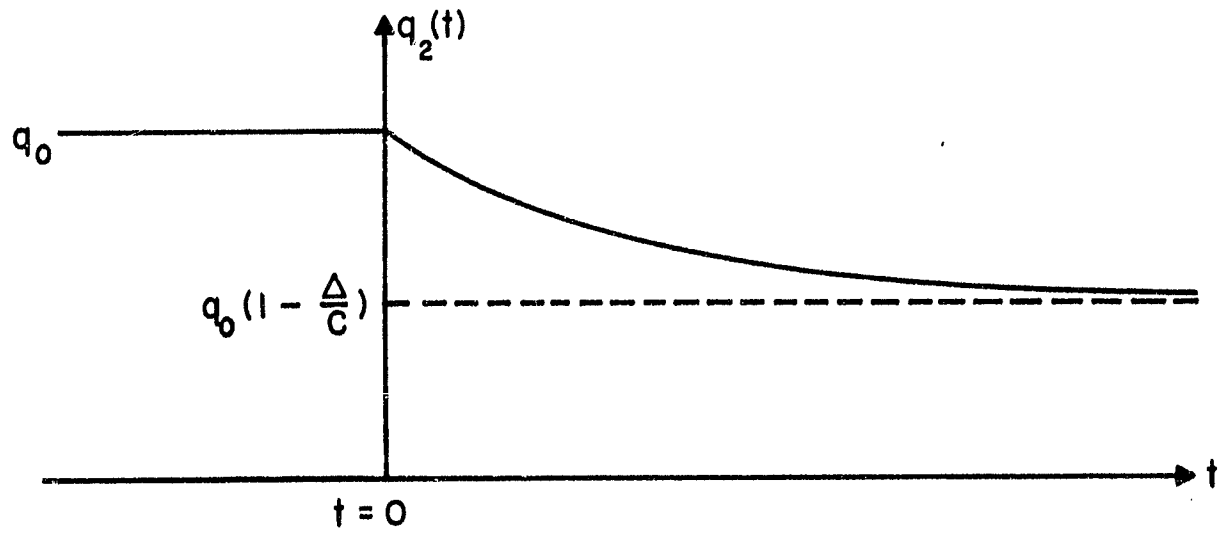

(b)

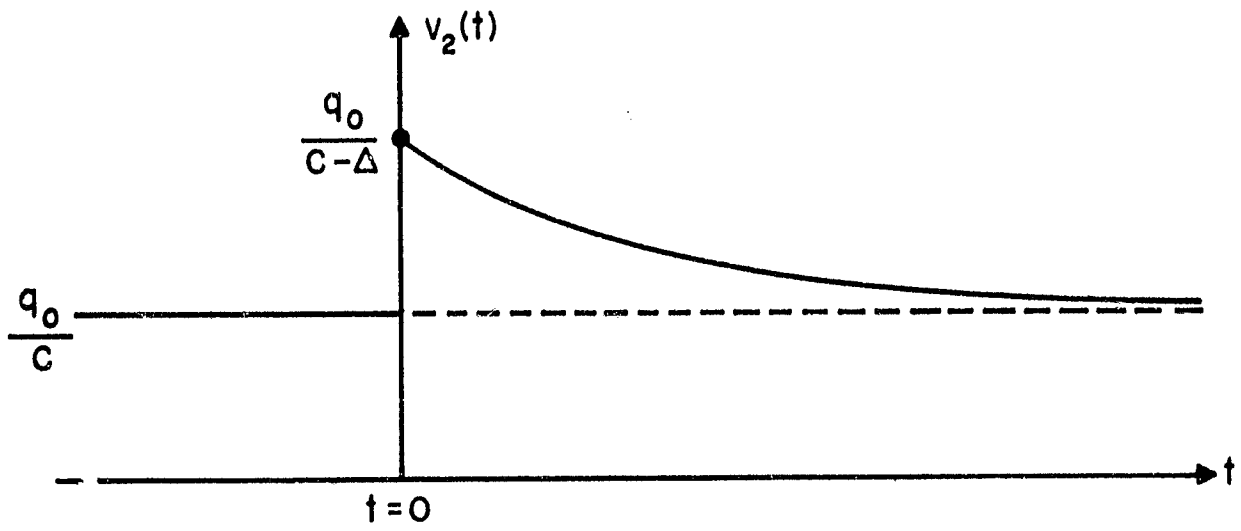

(c)

FIGURE 2 ELECTRICAL ANALOG FOR THE VACUUM SYSTEM OF FIGURE 1 AND RESPONSE TO SIMULTANEOUS CAPACITANCE CHANGES AT $t=0$

Taking Laplace Transforms where

$$f_2(s) \equiv L \left\{ q_2(t) \right\} ,$$

$$\left(sf_2 - q_0 \right) + \frac{2C}{R(C^2 - \Delta^2)} f_2 - \frac{1}{s} \left(\frac{2q_0}{R(C + \Delta)} \right) = 0.$$

Then

$$f_2(s) = \frac{q_0}{s + a} + \frac{\frac{1}{s} b}{s + a}$$

where

$$a \equiv \frac{2C}{R(C^2 - \Delta^2)} ,$$

$$b \equiv \frac{2q_0}{R(C + \Delta)} .$$

Now

$$L^{-1} \left\{ f_2(s) \right\} = q_2(t) = q_0 e^{-at} + \frac{2b}{a} e^{-at} \sinh \frac{a}{2} t ,$$

or

$$q_2(t) = q_0 \left(1 - \frac{\Delta}{C} + \frac{\Delta}{C} e^{-at} \right) , \quad t > 0.$$

This response is shown in Figure 2b.

In the circuit of Figure 2a the potential $v_2(t)$ taken with respect to ground is

$$v_2(t) = \frac{q_0}{C} , \quad t < 0$$

and

$$v_2(t) = \frac{q_0}{C - \Delta} \left(1 - \frac{\Delta}{C} + \frac{\Delta}{C} e^{-at} \right), \quad t > 0.$$

This response is shown in Figure 2c.

Using the previous discussion regarding the analogy between an electrical RC circuit and a vacuum system having molecular flow, we see from the solution for $v_2(t)$ that the absolute pressure in volume two in Figure 1 has the form

$$P_2(t) = P_0 \left(1 - \frac{\delta}{V} + \frac{\delta}{V} e^{-\alpha F t} \right) \tag{3}$$

for $t > 0$ if the volumes on both sides of the membrane are equal to V before the membrane movement, δ is the change in volume (volume one increases by the amount δ and volume two decreases by the amount δ), P_0 is the initial absolute pressure in volume two immediately after the membrane movement, F is the conductance of the membrane, and α is defined by

$$\alpha \equiv \frac{2V}{V^2 - \delta^2} .$$

Note that α depends upon δ to second order so that for small δ

$$\alpha \to \frac{2}{V} \quad \text{as} \quad \delta \to 0.$$

Therefore if δ is small, the system in Figure 1 has a response with time constant nearly $\frac{1}{2}VF^{-1}$ which is the time constant for a single-volumed system of volume $\frac{1}{2}V$ and the same flow conductance.

2.3 Application of Molecular Flow Theory to Analysis of a Gas Mixture

Equation (3) is the pressure response of two equal volumes connected by a conductance and containing a single gas at low pressure.

If the volumes are instantaneously changed as in the system in Figure 1, then the pressure equalizes exponentially if there is molecular flow through the conductance.

As discussed in Chapter I for a mixture of several species of gases flowing through the membrane, $P_2(t)$ in Equation (4) is a superposition of solutions (3) where the F_j are the various conductances and the X_j are weighting factors (molar fractions) to account for differing amounts of the N various species.

$$P_2(t) = \sum_{j=1}^{N} X_j \, S_j \, (t, F_j), \tag{4}$$

$$S_j \equiv P_0 \left(1 - \frac{\delta}{V} + \frac{\delta}{V} \exp \left[- \frac{2Vt}{V^2 - \delta^2} \, F_j \right]\right) \tag{4a}$$

with δ and V constants as defined above.

In order to determine the composition of a gas mixture using the system of Figure 1 we would solve a system of equations

$$P_2(t_i) = \sum_{j=1}^{N} X_j \, S_{ij} \, (t_i, F_j) \tag{5}$$

letting i = 1, 2, ... N and with S_{ij} determined from Equation (4a) at successive times t_i. The set of Equations (5) and (4a) is similar to Equation (2) but with the identification of time constant reciprocal

$$\lambda_j = \frac{2V}{V^2 - \delta^2} \, F_j \, .$$

To analyze a mixture of gases by molecular effusion through a membrane, the conductances F_j for molecular flow of the individual species must be determined as accurately as possible.

CHAPTER III

APPARATUS AND METHOD FOR MEASURING THE TIME CONSTANTS FOR EFFUSION OF VARIOUS GASES THROUGH MEMBRANES

3.1 Apparatus

It has been shown above that if the associated volumes and volume changes are known, the measurement of the conductance F_j of a membrane for a particular pure gas in the system of Figure 1 is equivalent to the measurement of the time constant for molecular effusion of the gas through the membrane to equalize pressure after some change in the volumes has occurred.

The apparatus which was basically that of Figure 1 consisted of a sintered silver or porous plastic (PVC) membrane mounted between two adjustable volumes. A Barocel (Datametrics, Inc.) electronic capacitance manometer type 1014 with a pressure-sensing head of type 511-10 was used for a pressure transducer.

One kind of membrane tested was made by Flotronics, Inc. of sintered silver particles with a hole size of 0.2μ and a thickness of 480μ giving a path-length to hole-size ratio of 240. The plastic membrane used was made by Millipore Corp. of polyvinyl chloride with a hole size of 10mμ and a thickness of 0.0135 cm, giving a path-length to hole-size ratio of 13,500.

3.2 Method of Measurement of the Time Constants

To determine the time constants of various pure gases effused through the membranes, an electrically generated (RC discharge) exponential was matched to the signal from the Barocel electronic manometer.

In the apparatus (Figure 1) the volumes were changed impulsively (in less than 0.1 second) and simultaneously by movement of the membrane M from position A to B. The flexible bellows enclosing the volumes on either side of the membrane allowed this movement which created an instantaneous pressure difference across the membrane. This pressure difference then equalized with an exponential or nearly exponential waveform in time as the gas effused through the membrane.

In Figure 3 which is the block diagram of the circuitry, the microswitch was closed by the membrane assembly movement. Then the Barocel and RC-generated exponential signals were connected simultaneously by the relay #1 having a variable time delay. The purpose of the time delay is explained in Section 3.4

Exponentials of various peak heights and time constants were generated by the circuit of Figure 4 to find the exponential that matched the pressure response curve. When the difference between the RC discharge and the Barocel signal was a straight line at zero plotted in time on the strip chart recorder, then the time constant could be determined to a high degree of accuracy from the resistance-capacitance product in the circuit of Figure 4.

Signals of the form

$$A_0\left[\exp\left(-\frac{t}{\tau}\right) - \exp\left(-\frac{t}{\tau'}\right)\right]$$

with A_0 = 3 volts

will have a value of about one mv for

$$5 \text{ sec} < t < 25 \text{ sec}$$

if

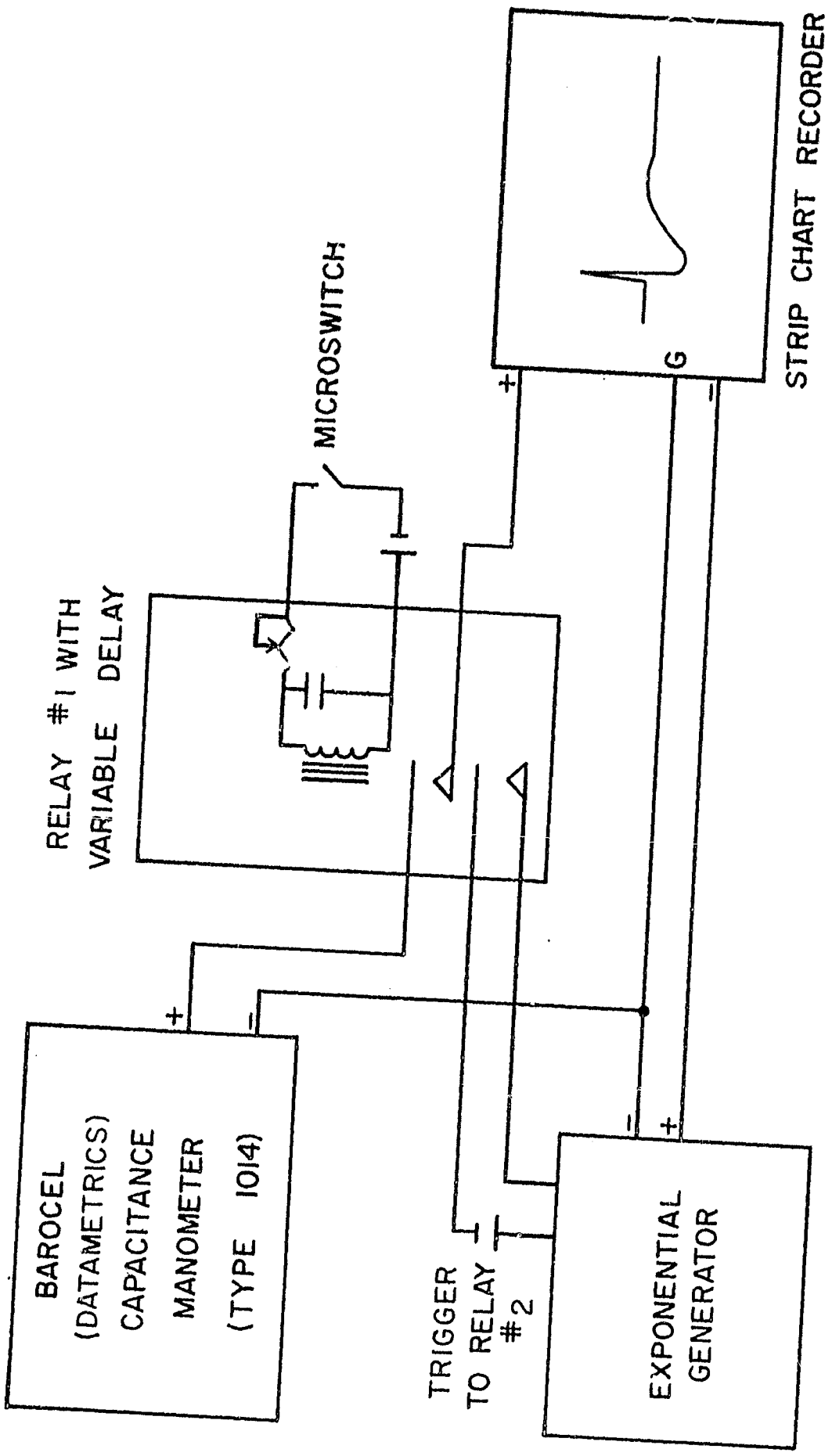

FIGURE 3 BLOCK DIAGRAM OF CIRCUITRY FOR TIME CONSTANT MEASUREMENTS

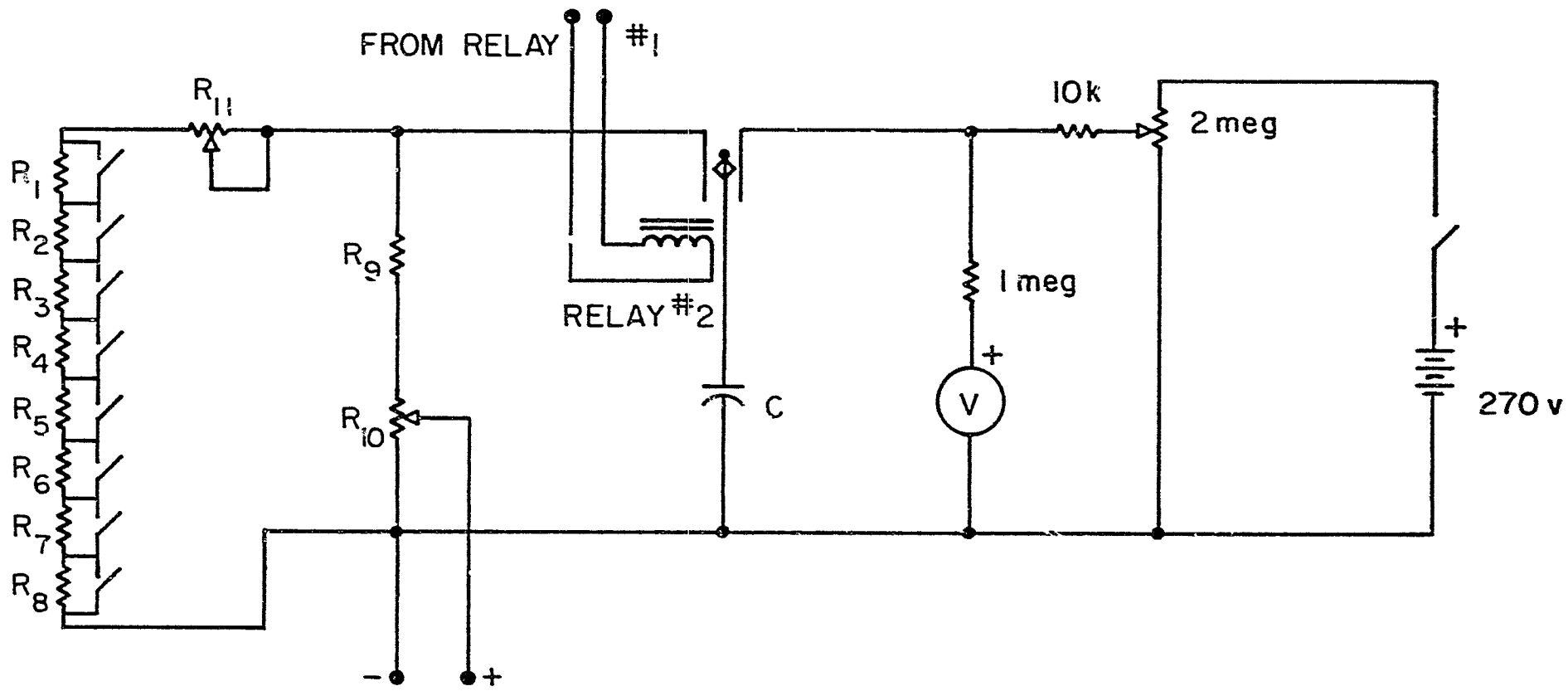

$R_1 = 100{,}950 \pm 100\,\Omega$ $R_7 = 2.006\,\text{meg} \pm 1\text{k}$

$R_2 = 149{,}800 \pm 100\,\Omega$ $R_8 = 3.001\,\text{meg} \pm 1\text{k}$

$R_3 = 200{,}700 \pm 100\,\Omega$ $R_9 = 9.135\,\text{meg} \pm 5\text{k}$

$R_4 = 319{,}900 \pm 100\,\Omega$ $R_{10} = 260{,}200 \pm 100\,\Omega$

$R_5 = 700{,}600 \pm 200\,\Omega$ $R_{11} = 100\text{k}$, WIREWOUND

$R_6 = 1.011\,\text{meg} \pm 500\,\Omega$ $C = 9.15\,\text{mfd} \pm .3\%$

FIGURE 4 EXPONENTIAL GENERATING CIRCUIT FOR MEASUREMENT OF TIME CONSTANTS

$$\tau'/\tau = 1.001$$

when

$$10 \text{ sec} < \tau < 30 \text{ sec.}$$

Thus, under these conditions we can detect a 0.1% difference in time constant between two exponentials if we can observe a one mv voltage difference over the middle of the decay from 5 to 25 seconds. The necessity for accurate absolute voltage measurements is eliminated by this null method.

The pressure range investigated was 1 to 100 Torr, and the peak pressure signal voltages were maintained between two and five volts by adjusting the range on the pressure transducer. The peak pressure increase was about four percent.

The values of the resistors in Figure 4 were determined on a Wheatstone bridge. The total resistance was calculated by combining in parallel the branch containing the resistors R_1 to R_8 and R_{11} with the branch containing R_9, R_{10} and the input impedance of the strip-chart recorder. The method of calculation of the resistance of each branch is obvious from Figure 4.

3.3 Accurate Determination of the Capacitance in Figure 4

Since the capacitance in the circuit of Figure 4 was not changed (the variation in time constant was obtained by resistance changes), a special effort was made to measure the capacitance accurately so that the RC products could be immediately calculated once R had been determined.

The va'ue of the capacitance in Figure 4 was determined by a least square fit to 10 RC decays at each of three different resistances. The averages of the 10 capacitance determinations at each resistance were 9.13 mfd, 9.16 mfd, 9.18 mfd. Therefore the value of 9.15 $\pm$ 0.03 mfd was used; however, the considerations associated with measurements of capacitance to this accuracy need to be mentioned. These considerations are temperature and voltage coefficients, leakage resistance and dissipation factor. A DC-equivalent circuit for a real capacitance is shown in Figure 5 in which R_L is the leakage resistance and R_D is the dissipation resistance.

The capacitors used were paper-mylar types, and these have small enough temperature coefficients not to be affected by normal variations in room temperature. Their voltage coefficient is essentially nil, and the insulation resistance is above 10^4 meg, also having a negligible effect. The leakage resistance of this type of capicator is usually measured in the thousands of megohms, and it was measured and found to be above 10^4 meg.

However, the dissipation factor can be as high as 0.3% with this type of unit. Figure 5 shows a plot of R_TC versus R (R is a real resistor) where R_T is the total effective resistance ($R_T \tilde{=} R + R_D$) and the R's were measured independently. If $R_D > 0$ then $R_TC > 0$ for $R = 0$, but a calculated least-square fit showed that $R_D < 3K$ which can be neglected. Therefore we feel correct in assigning the value of 9.15 mfd $\pm$ 0.3% to the capacitance.

One could simply use the same capacitor for all determinations of the time constants for various gases, and then we would hope to

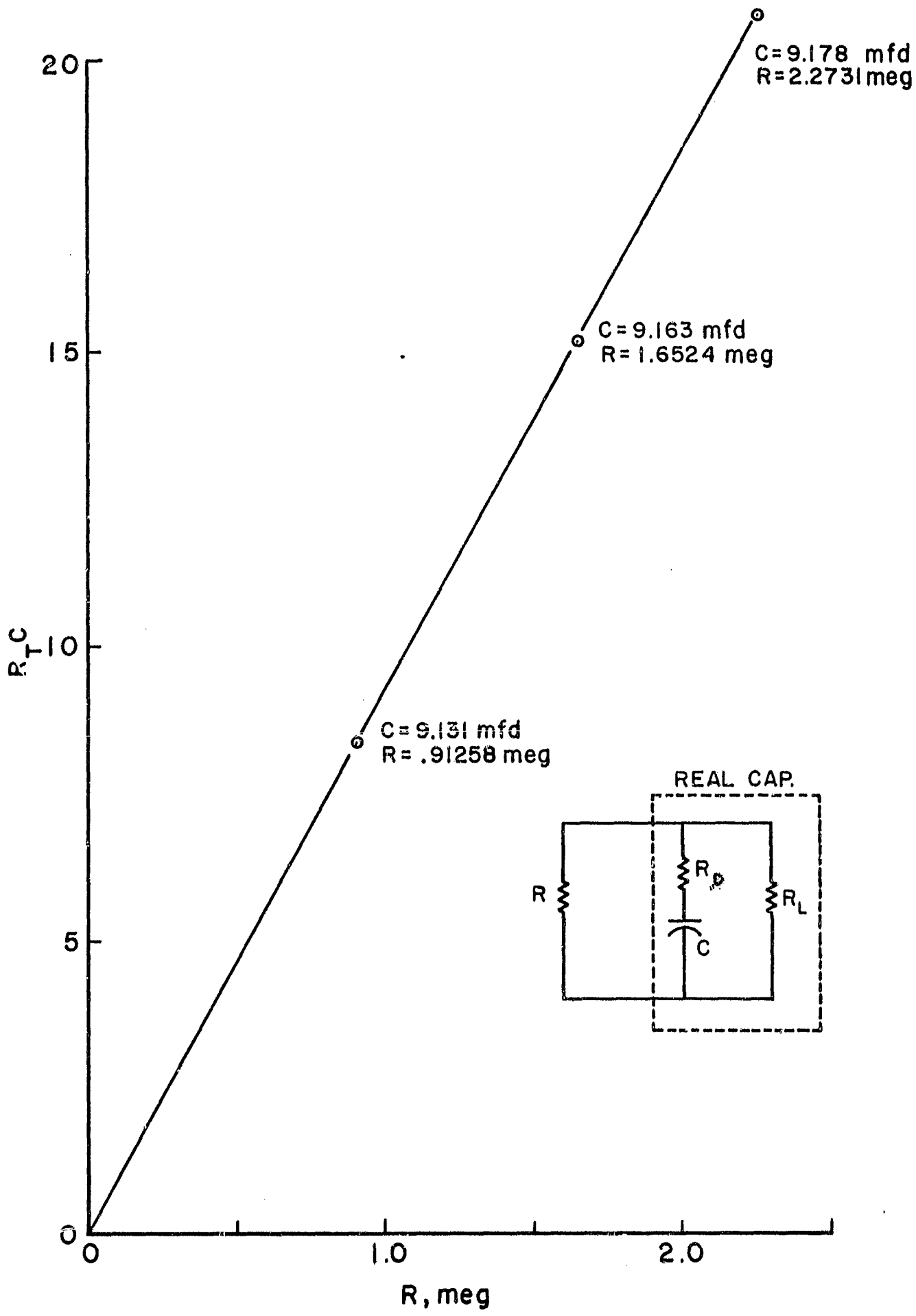

FIGURE 5 PLOT OF R VERSUS R_TC

obtain relative time constants consistent within about 0.1%, which is approximately the accuracy of the pressure transducer. Determination of the capacitance allows the specification of the time constants in seconds, and, hence, the calculation of the absolute conductance values of the membrane for various gases (if the associated volumes and volume changes are known).

3.4 Temperature Transient Effects

Transient temperature effects will cause the pressure vs time curve discussed previously to be non-exponential. If P_1, V_1, T_1 and P_2, V_2, T_2 are the initial and final pressure, volume and temperature, respectively, then

$$\frac{P_1}{P_2} = \frac{T_1 V_2}{T_2 V_1} = \left(\frac{V_2}{V_1}\right)^{\gamma}$$

$$T_2 = T_1 \left(\frac{V_1}{V_2}\right)^{\gamma - 1}$$

for adiabatic change where γ is the ratio of specific heats for the gas. Taking $V_2 = 0.96V_1$ and $T_1 = 300°K$ and $\gamma = 1.5$ then $T_2 = 306°K$.

It must be determined how seriously this heating will affect the time constant determinations. How long does the transient last and how is the transient affected by pressure and the species of gas?

The circuit used for transient temperature measurements is shown in Figure 6. It consisted of three parts: a constant current source, a fast-acting thermistor, and a fast strip-chart recorder.

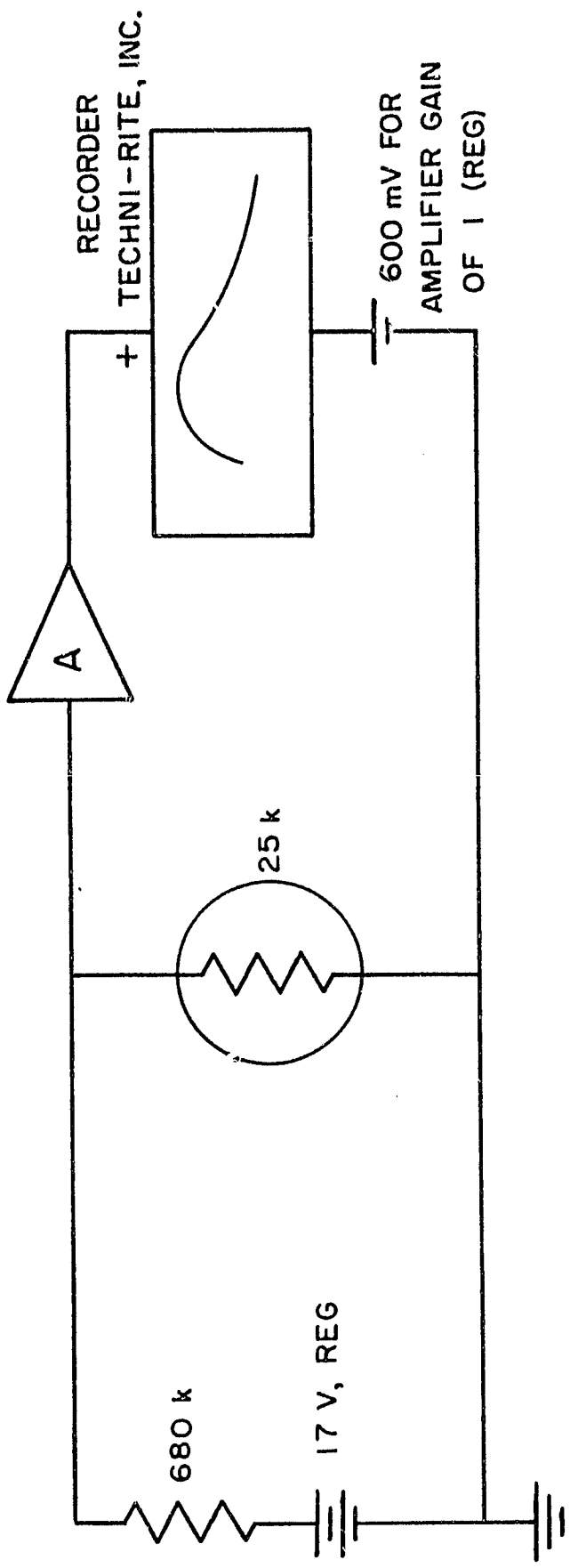

FIGURE 6 CIRCUIT FOR TEMPERATURE TRANSIENT MEASUREMENTS USING A FAST THERMISTOR

The current source produced a drop of 600 mv across the thermistor at room temperature, and any change in resistance of the thermistor was shown immediately as a change in voltage drop which was measured by the strip-chart recorder. The amplifier A provided a high impedance input as well as range changes, and the 600 mv supply offset the 600 mv drop across the thermistor at room temperature.

The thermistor was a VECO Corp. "Micro Bead" with a time constant of 0.12 sec. in air at one atmosphere and 25°C according to the manufacturer. The thermistor was placed inside the bellows assembly about three-eights of an inch from the membrane. The strip-chart recorder was a Techni-Rite Inc. model TR-711 which can follow over 100 Hz.

Figure 7a shows the temperature waveforms for three gases effused through the sintered silver membrane having 0.2μ holes at pressures of 90 Torr or above. Xenon shows the highest peak and the longest duration which is due to its slower molecular velocity. Even for Xenon the transient is essentially over within one second. Hence it was concluded that the temperature transients may be neglected after one second.

The purpose of the relay #1 in Figure 3 having a variable time delay was to delay about one second after the bellows movement before connecting the two waveforms to be compared. In this way transient temperature effects in the first second of the pressure waveform were ignored.

Figure 7b shows the peak temperature recorded from waveforms like those of Figure 7a for several gases at various pressures. Note

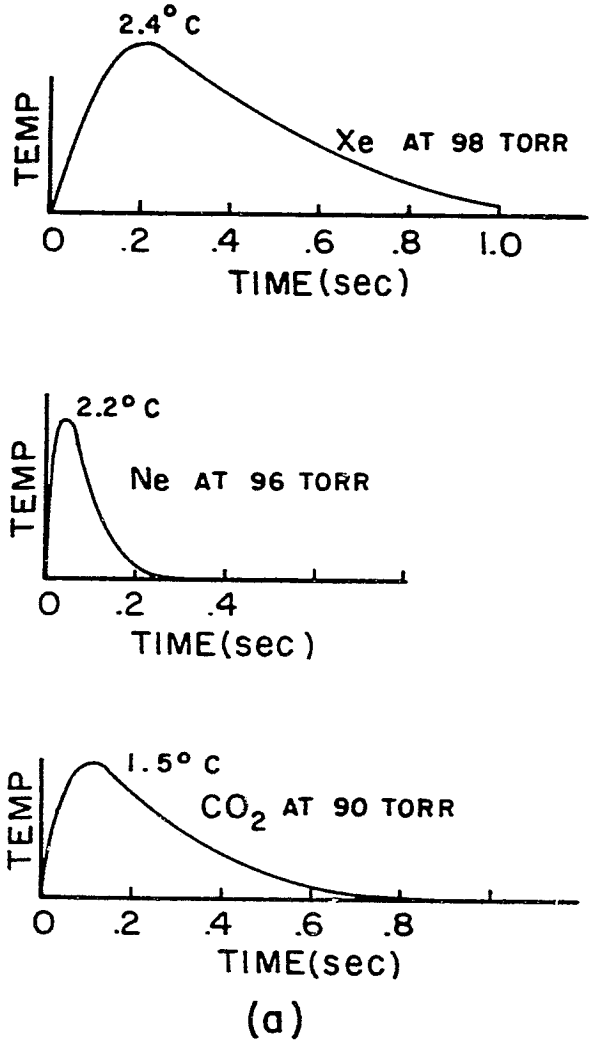

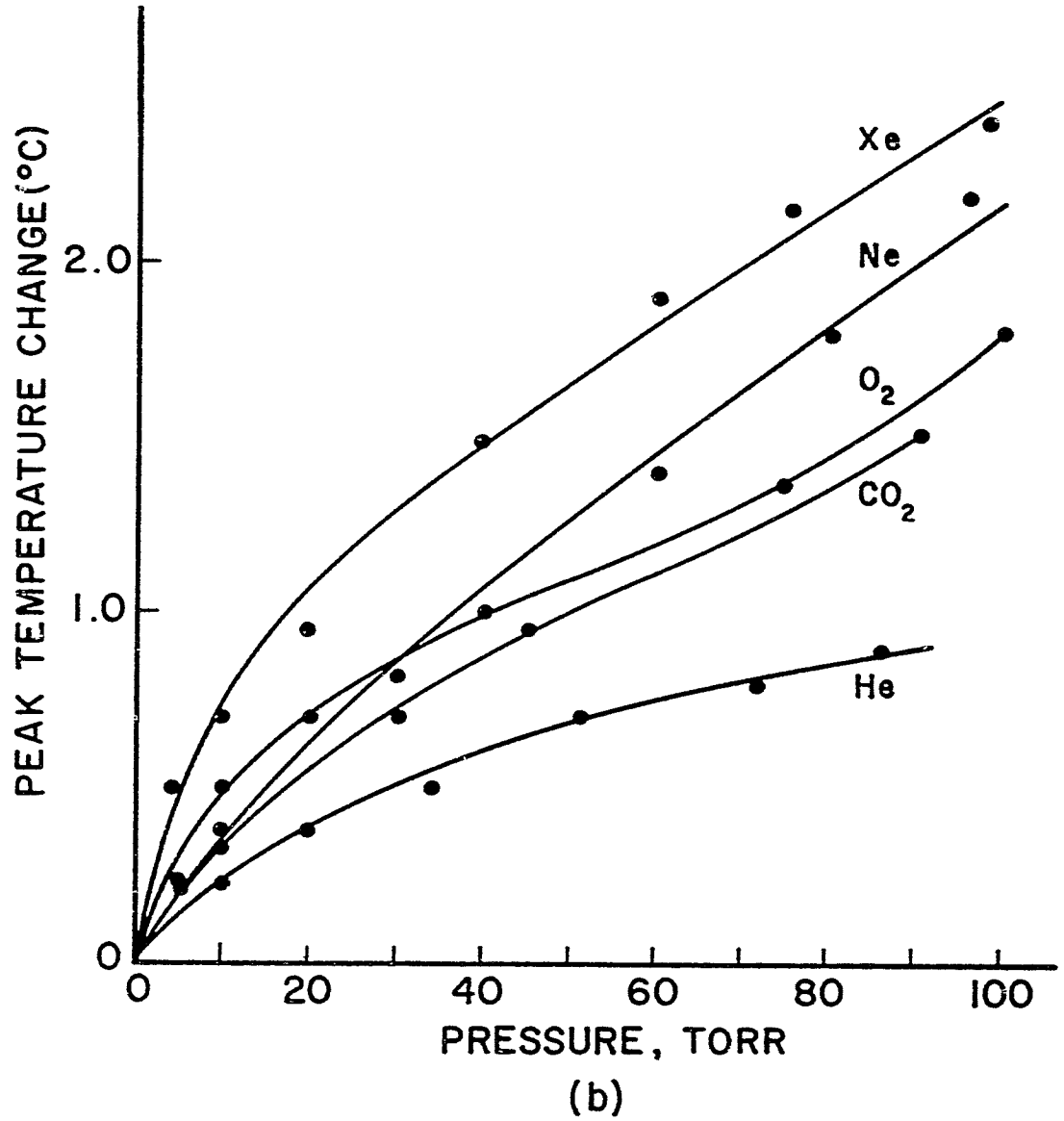

FIGURE 7 TEMPERATURE TRANSIENT EFFECTS FOR VARIOUS GASES, 28°C

that the curves for the two inert gases xenon and neon ($\gamma \cong 1.65$) are grouped together as are the curves for O_2 and CO_2 ($\gamma \cong 1.35$). Helium showed smaller temperature rises because of its very high conductivity.

That the time constant of the thermistor should be a function of pressure can be seen by comparing the mass of gas hitting the very small thermistor (0.013 cm diameter) and two wires connecting the thermistor (0.0018 cm diameter, 0.64 cm length) within 0.1 second after the compression (which is approximately the time to peak of the temperature waveforms) with the mass of the thermistor plus wires (weighed as well as calculated to be about 0.1 mg).

From Dushman (1962) the mass G of gas striking a surface is

$$G = 5.833 \times 10^{-2} \times \left(\frac{M}{T}\right)^{1/2} P_T \text{ g cm}^{-2} \text{ sec}^{-1}$$

where M is the gram molecular weight, T the Kelvin temperature, P_T the pressure in Torr. If M = 10, T = 300°K, the area of the thermistor plus wires is 76×10^{-4} cm^2, then the mass of gas striking the thermistor and wires in 0.1 second is

$$G \cong 1.5 \times 10^{-2} P_T \text{ mg}.$$

The mass of gas striking the thermistor and wires within 0.1 second after the compression is linear with pressure and within one order of magnitude of the mass of the thermistor plus wires from about 1 to 75 Torr. This fact accounts for the behavior shown in Figure 7b in which the peak temperature changes with pressure from 1 to 100 Torr which is consistent with the results given by Dushman (1962) on page 45.

The fact of the pressure-dependent thermistor time constant in no way affects the conclusion that the temperature transients are essentially over within one second. It can be seen that if the declining waveforms for t > 0.2 second of Figure 7a were projected back to the time origin, the peak temperature rises would be about 4 to 6°C as calculated.

CHAPTER IV

RESULTS OF EXPERIMENTAL MEASUREMENTS

4.1 Exponential Pressure Response of the System

The time constants for effusion of gases through a single membrane were measured by the method of Chapter III.

Figure 8 shows the pressure vs time curve for argon at one Torr, and four curves which are the differences between the pressure response and an exponential generated by the circuit of Figure 4 at different values of R_{11}. The resistors R_2, R_3 and R_7 were used in series with each of these four values of R_{11}. The top curve shows that the zero point drifted about 0.8 mv in 30 seconds. From the curves shown in Figure 6 we would deduce a value of 45 ± 1k for R_{11}. The total resistance was calculated by combining $R_2 + R_3 + R_7 + R_{11}$ in parallel with the resistance of the branch containing R_9, R_{10} and the input impedance of the strip-chart recorder.

According to the manufacturer the accuracy of the pressure transducer is better than 0.1% (limited primarily by diaphragm memory). Small ambient temperature variations are also a problem when measuring pressure differences to less than one percent.

With the system thermally insulated and using the curve-matching approach, the time constants for various gases were calculated to be proportional to the square root of molecular weight within one part in eight hundred as shown in Figure 9.

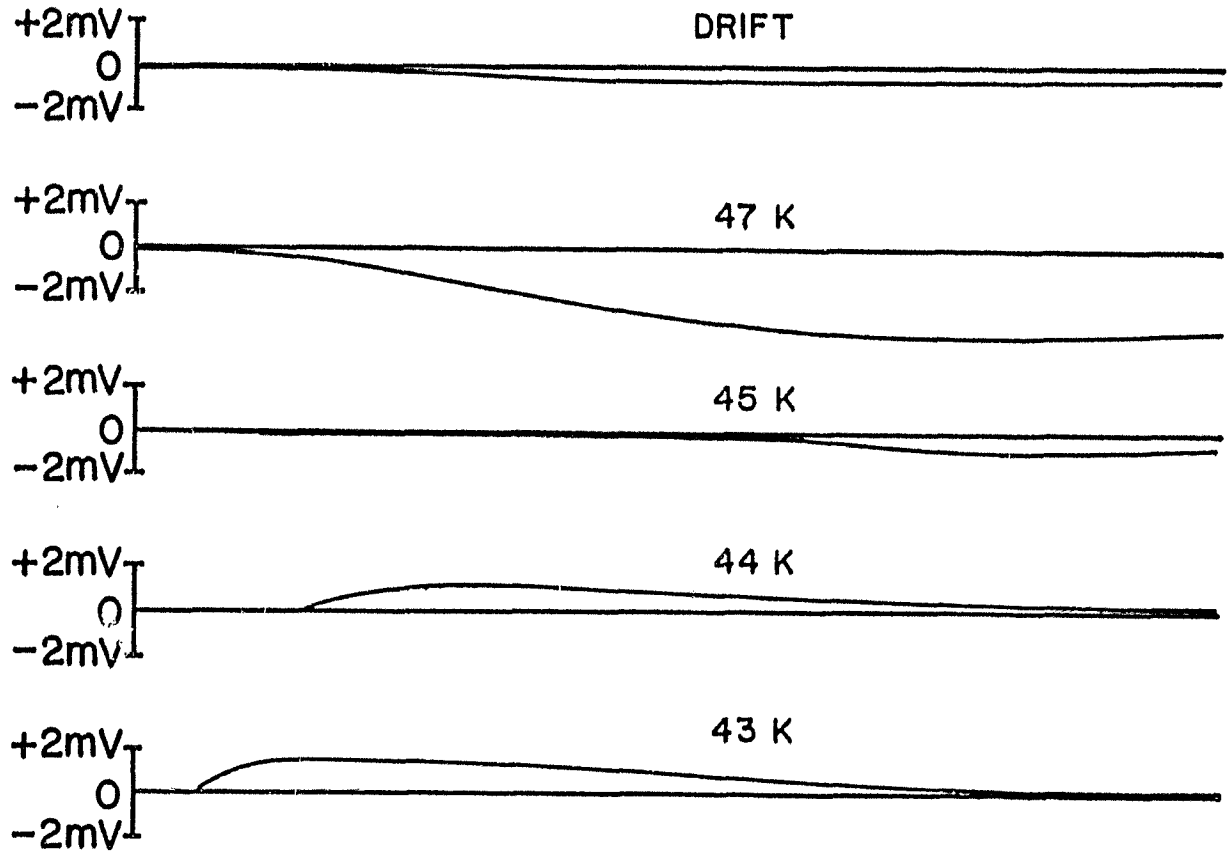

FIGURE 8 ARGON PRESSURE RESPONSE AT ONE TORR. ABOVE ARE THE DIFFERENCES BETWEEN THE ARGON PRESSURE RESPONSE AND RC DECAYS FROM THE CIRCUIT OF FIGURE 4 AT VARIOUS VALUES OF R_{11} IN SERIES WITH 2.346 MEG

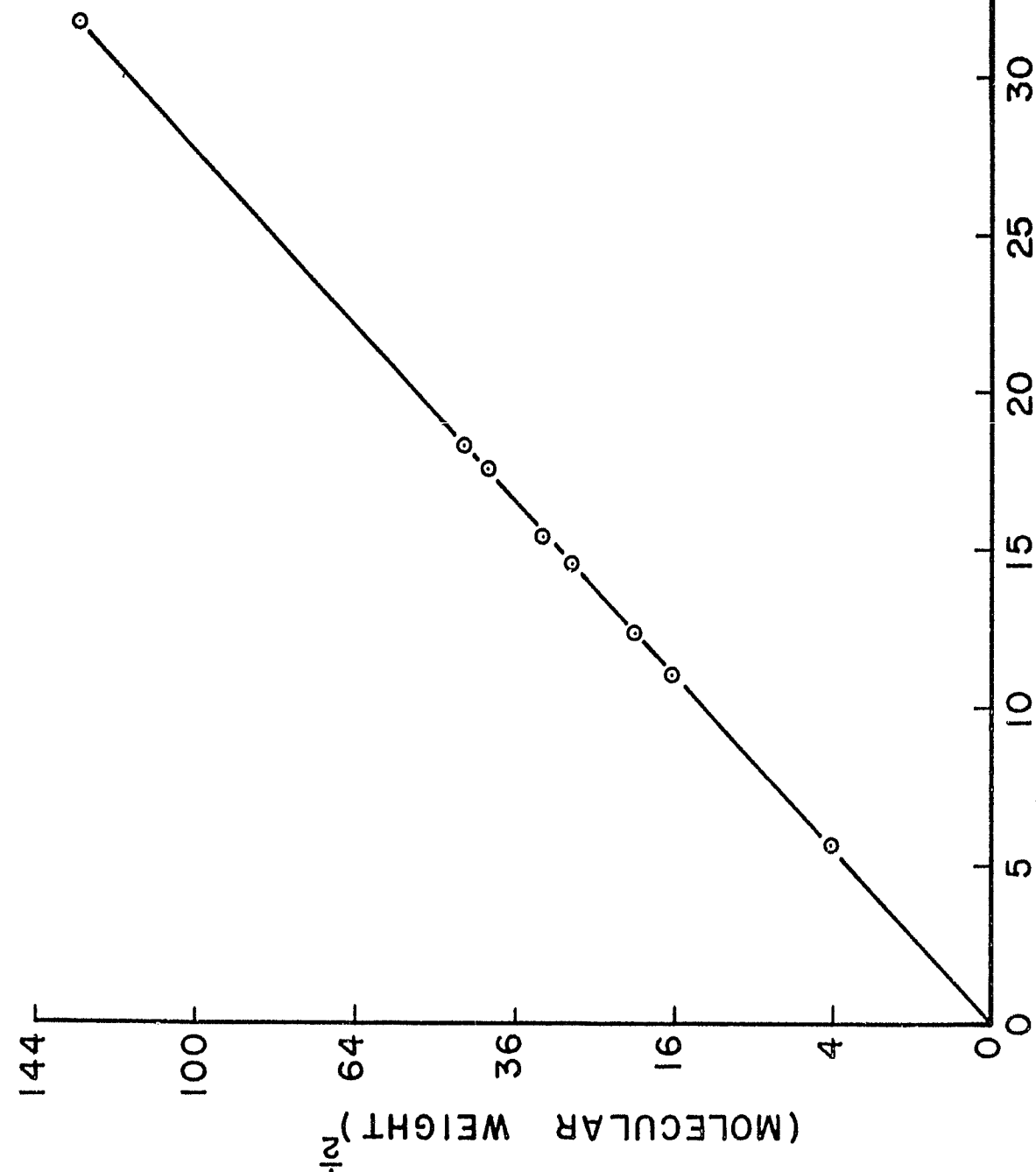

FIGURE 9 SQUARE ROOT OF MOLECULAR WEIGHT VERSUS TIME CONSTANT AT 28°C, ONE TORR

4.2 Results of Time Constant Measurements

Figure 10 shows time constants for effusion of various pure gases through a membrane of sintered silver particles having holes no larger than 0.2μ. For a particular pure gas molecular flow takes place at pressures for which the time constant is independent of pressure. For the heavier gases the time constants decrease above about 10 Torr due to viscous effects, although the responses appear exponential well beyond 10 Torr except for Xenon which shows a non-exponential waveform above 11 Torr.

The requirement usually cited for molecular flow is that

$$L/d > 1 \qquad (6)$$

where L is the mean free path of the gas and d is a characteristic dimension. If the hole size of 0.2μ is taken as the characteristic dimension for the data of Figure 8, then the molecular flow condition (6) above gives the result that we would expect molecular flow to pressures above 200 Torr. However, condition (6) is only an approximate criterion for molecular flow.

Since the time constants in Figure 10 are only strictly pressure independent up to about 10 Torr, this would imply a condition for molecular flow

$$L/d > 20.$$

The measurements of Knudsen (1909), with about one percent accuracy, on molecular flow through diaphragms of platinum foil of thickness 0.0025 mm and 0.0050 mm with holes of 5.21×10^{-6} cm^2 and

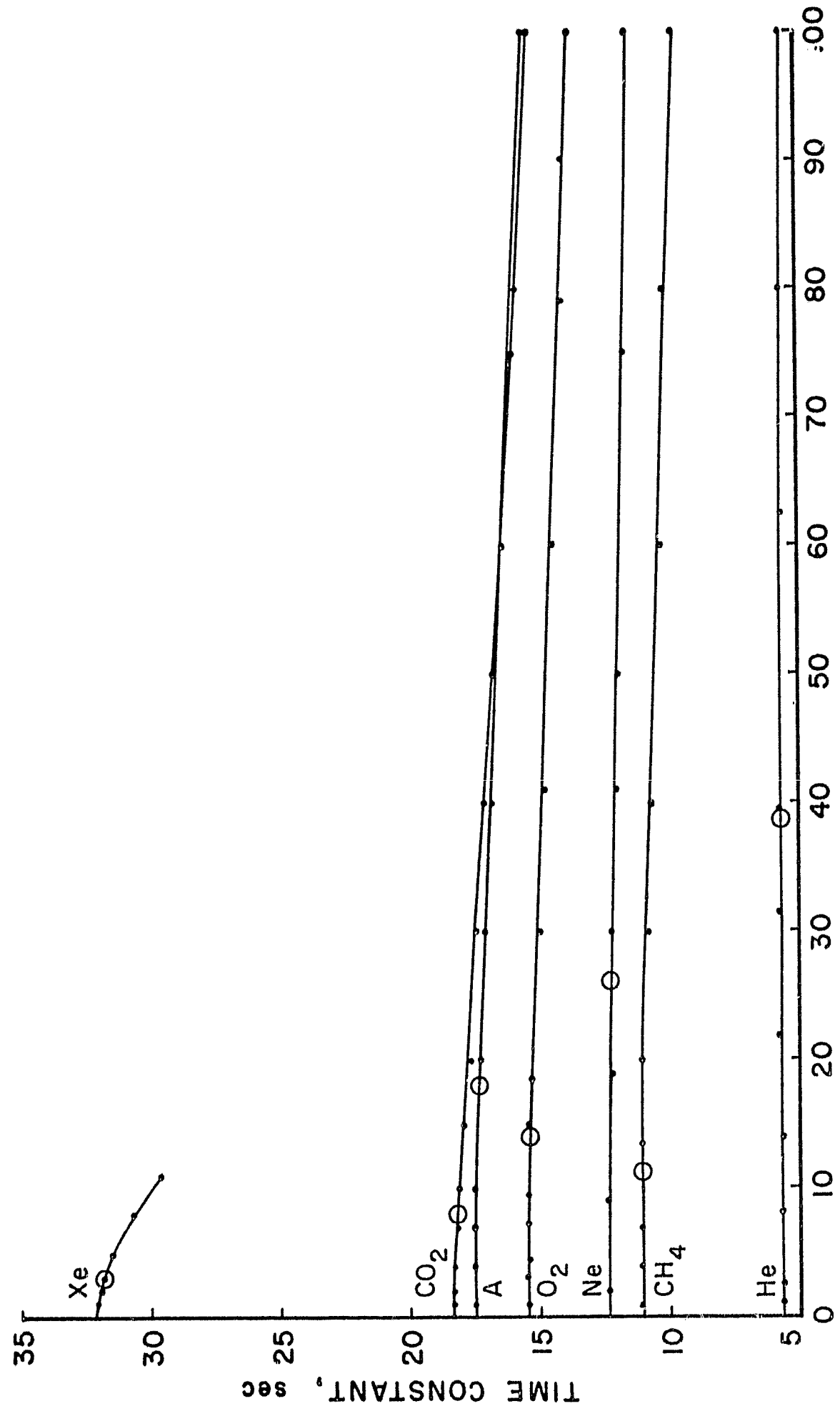

FIGURE 10 TIME CONSTANTS FOR VARIOUS GASES FLOWING THROUGH .2μ-HOLE MEMBRANE AT 28°C

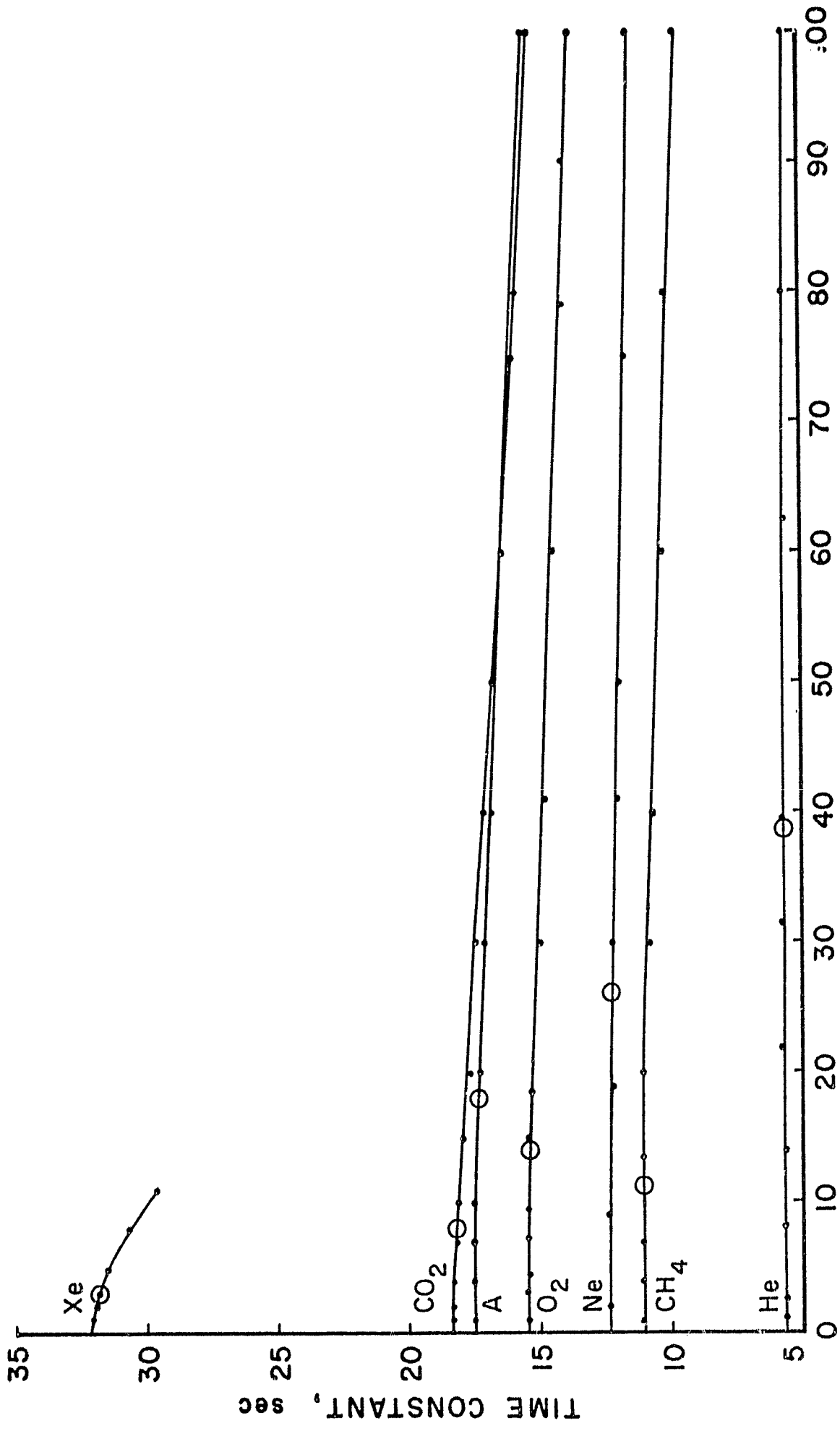

FIGURE 10 TIME CONSTANTS FOR VARIOUS GASES FLOWING THROUGH .2μ-HOLE MEMBRANE AT 28°C

66.0×10^{-6} cm^2 area, respectively, showed molecular flow continuing to L/d = 10. The data shown here for much smaller holes (3×10^{-10} cm^2 area) and having higher accuracy are consistent with those results of Knudsen.

The circles in Figure 10 show the pressures for various gases at which L/d = 20 calculated from the well known relation (Dushman, 1962)

$$L = 8.589 \frac{\eta}{P} \left(\frac{T}{M} \right)^{1/2}$$

where η is the viscosity in poises, P is the pressure in Torr, T is the Kelvin temperature and M is the molecular weight in grams.

Figure 11 exhibits data similar to that of Figure 10 except that it was taken using a porous plastic (PVC) membrane with hole size 10mμ. From condition (6) holes of this size should give molecular flow up to 4000 Torr, however, the time constants are pressure independent to the accuracy of Figure 10 only to about 20 Torr. For Figure 11 L/d = 20 occurs around 200 Torr.

Figures 12, 13 and 14 show the percent of decrease from the time constant at one Torr for three representative gases at pressures above one Torr. In the three figures notice that for the curves taken above room temperature the percentage difference of time constant from the value at one Torr is smaller at all pressures than for the curves taken at room temperature. The membrane having 10mμ holes shows only about one-third to one-half the change of the time constant that the silver membrane showed from 1 to 100 Torr.

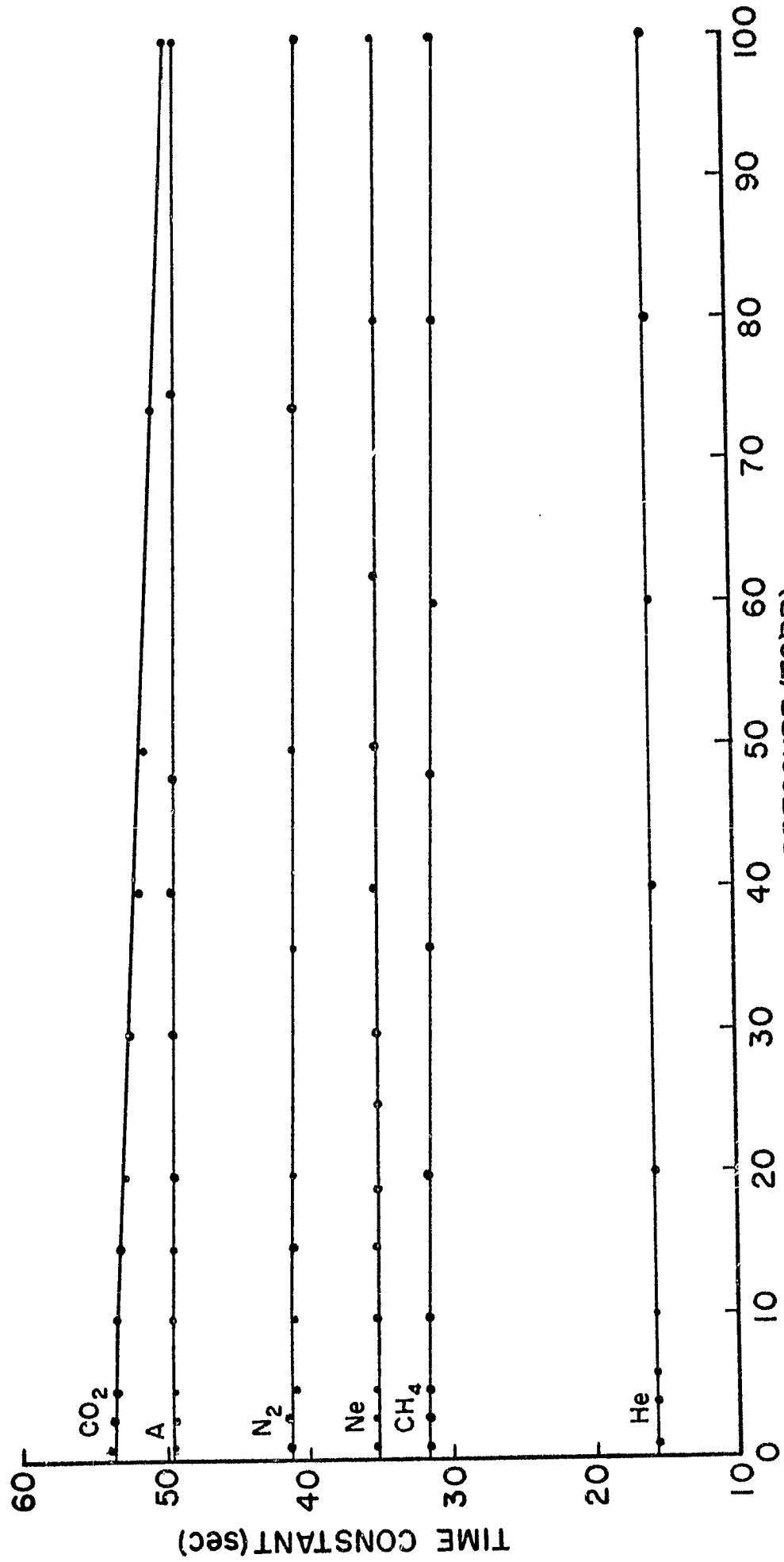

FIGURE 11 TIME CONSTANTS FOR VARIOUS GASES FLOWING THROUGH 0.01μ-HOLE MEMBRANE AT 30°C

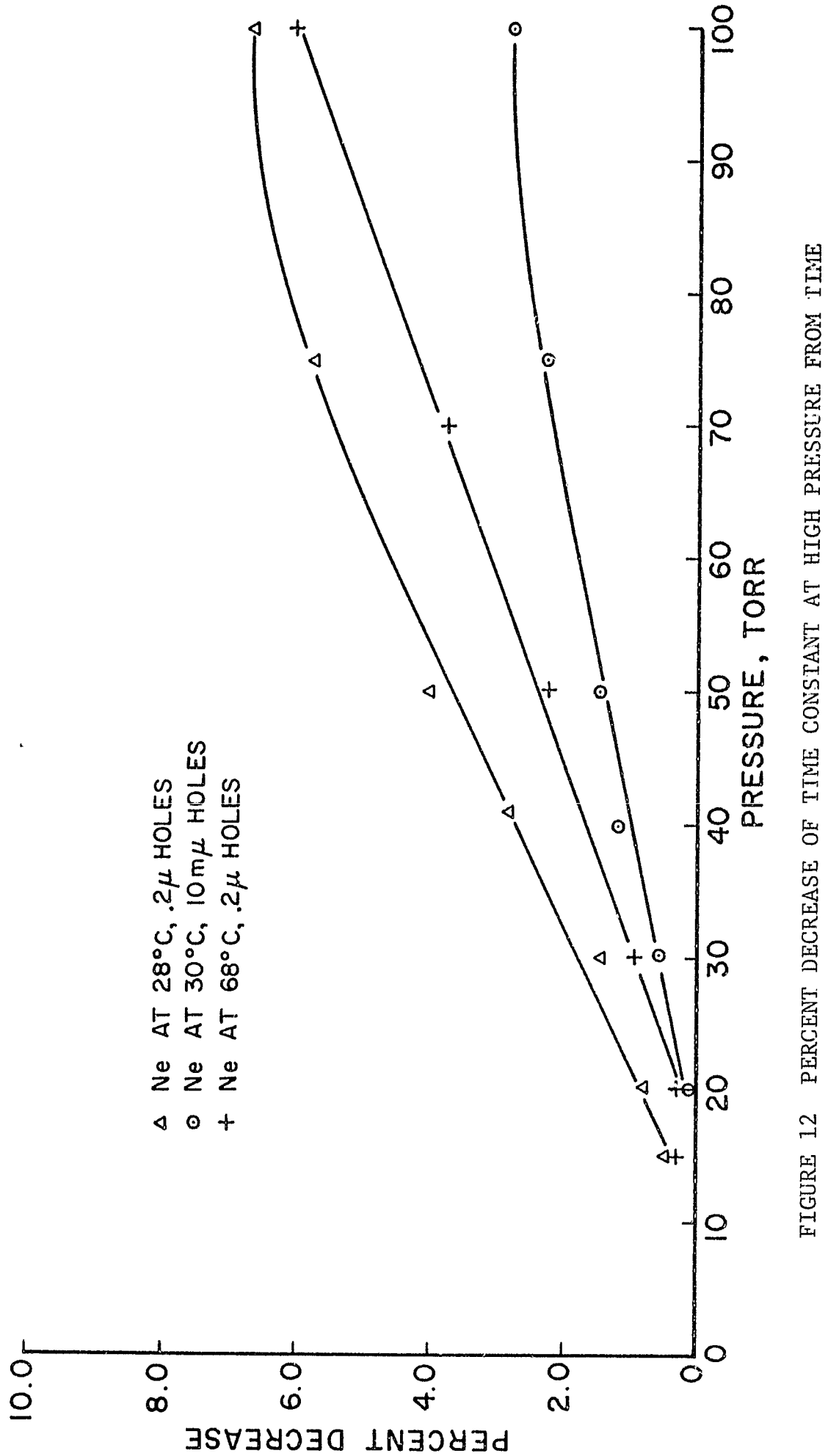

FIGURE 12 PERCENT DECREASE OF TIME CONSTANT AT HIGH PRESSURE FROM TIME CONSTANT AT ONE TORR FOR NEON

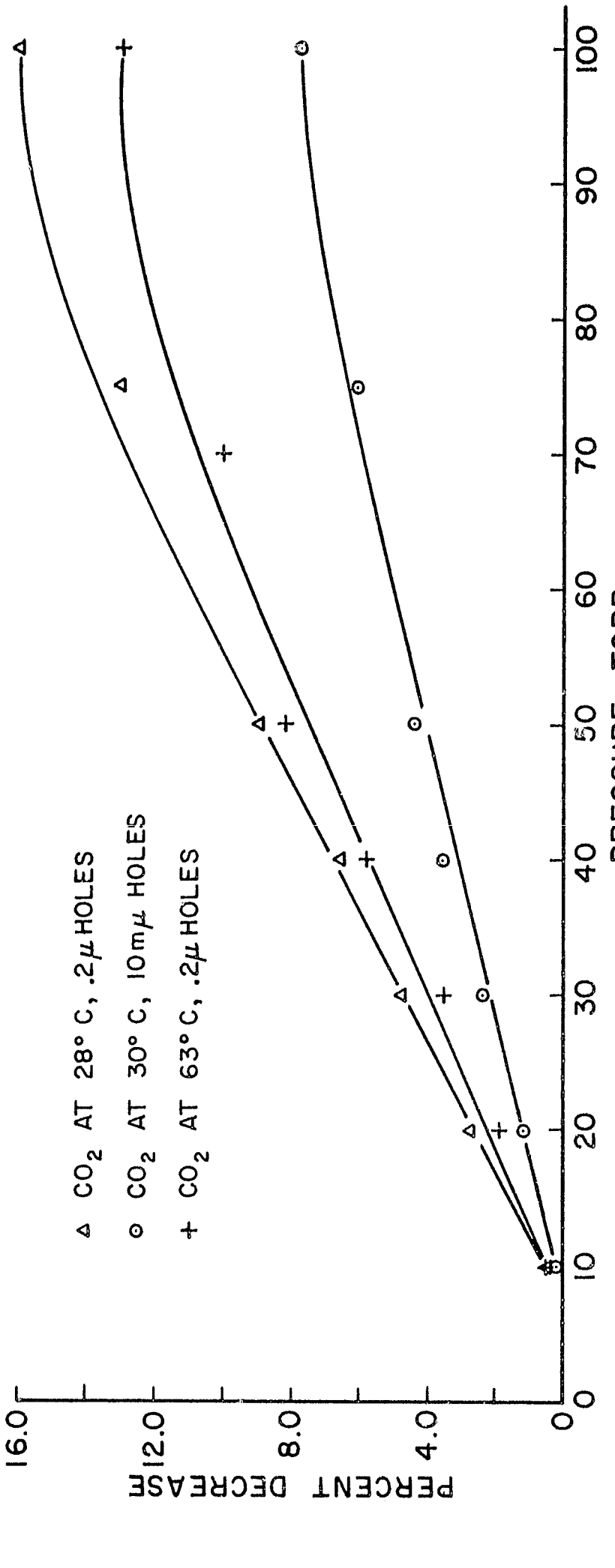

FIGURE 13 PERCENT DECREASE OF TIME CONSTANT AT HIGH PRESSURE FROM TIME CONSTANT AT ONE TORR FOR CARBON DIOXIDE

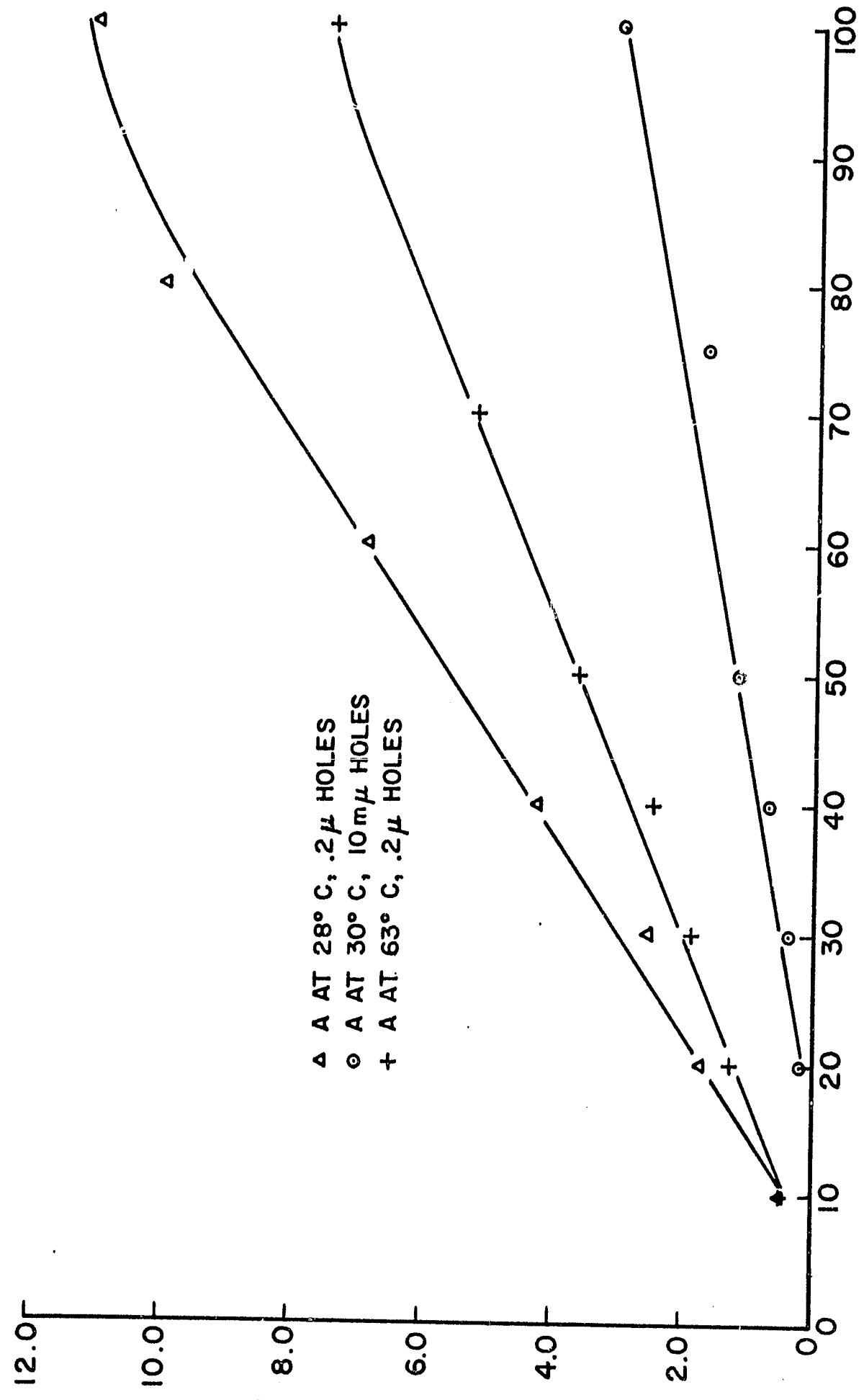

FIGURE 14 PERCENT DECREASE OF TIME CONSTANT AT HIGH PRESSURE FROM TIME CONSTANT AT ONE TORR FOR ARGON

4.3 Measurement of Membrane Conductance

As discussed above, the determination of the time constant for molecular effusion of a pure gas through a membrane or other conductance is equivalent to a determination of the value of the conductance itself, if the values of associated volumes are known.

Steckelmacher (1966) has pointed out the difficulties in calculating conductances, either from Clausing's integral equations, or by the method of Oatley (1957), or with Monte Carlo methods (eg. Smith and Lewin, 1966).

Two previous experimental methods noted by Steckelmacher (1966) which require accurate gas flow or angular distribution measurements are also difficult. Ruthberg (1964) has done elaborate determinations of conductances to within one percent using substitution procedures.

The accurate determination of time constants as shown here provides a method with almost 0.1% accuracy for the experimental measurements of the conductance of a membrane to molecular flow.

CHAPTER V

POSSIBILITY OF ANALYSIS OF GAS MIXTURES BY VACUUM NETWORKS: DATA PROCESSING CONSIDERATIONS

5.1 Use of the Results of Chapter IV and Least-Square Fits

It has been suggested by Kendall (1966) and Kendall and Pulfrey (1968) that there are several important advantages to a system which could analyze gas mixtures on the basis of the different conductances of a membrane for molecular effusion of pure gas species. Among these advantages are the complete elimination of the necessity for production, acceleration, focussing and detection of ions; the elimination of chemical changes caused by electron bombardment; and the capability of operation at relatively high pressures.

In the previous chapter it has been shown for two types of membranes that below certain pressures the conductances of the membranes are constant for a particular gas. Further it was demonstrated that for pressures low enough that the conductances were pressure independent, the conductances varied inversely as the square root of the molecular weight of the gas.

Because of these facts the analysis of a gas mixture by molecular effusion as suggested in Chapter I is a practical possibility.

The solution of the system of Equations (2)

$$P(t_i) = P_0 \sum_{j=1}^{N} X_j \, e^{-\lambda_j t_i} \qquad (2)$$

is difficult because even the smallest errors in the data are sufficient to cause large errors in the solutions. Therefore a better approach is to make a minimum-square fit of the known exponentials to the data

curve using several times as many data points as the number of gases pre ent.

We write the squared deviation D between a fitted waveform $P_0 \sum_{j=1}^{N} X_j \, e^{-\lambda_j t_i}$ and a set of data points $P(t_i)$ as

$$D \equiv \sum_{i=1}^{M} \left(P(t_i) - \sum_{j=1}^{N} X_j \, B_{ij} \right)^2 ,$$

$$B_{ij} \equiv P_0 \, e^{-\lambda_j t_i} \qquad (7a)$$

where N is the number of gases in the mixture, M is the number of data points taken, and the unknowns X_j are the molar proportions of the j^{th} gas species present.

Rewriting the expression above for D gives

$$D = \sum_{i=1}^{M} P(t_i)^2 - 2 \sum_{i=1}^{M} P(t_i) \sum_{j=1}^{N} X_j \, B_{ij} + \sum_{i=1}^{M} \left(\sum_{j=1}^{N} X_j \, B_{ij} \right)^2 .$$

Differentiating D with respect to a particular unknown X_J, and setting $\frac{\partial D}{\partial X_J} = 0$ yields

$$\frac{\partial D}{\partial X_J} = -2 \sum_{i}^{M} P(t_i) \, B_{iJ} + 2 \sum_{i=1}^{M} \left(\sum_{j=1}^{N} X_j \, B_{ij} \right) B_{iJ} = 0,$$

$$\sum_{i=1}^{M} P(t_i) \, B_{iJ} = \sum_{i=1}^{M} \sum_{j=1}^{N} X_j \, B_{ij} \, B_{iJ} ,$$

$$\sum_{i=1}^{M} P(t_i) \, B_{iJ} = \sum_{j=1}^{N} X_j \left(\sum_{i=1}^{M} B_{ij} \, B_{iJ} \right) . \qquad (7)$$

Let (7) define the first N-1 equations of a linear system to determine the X_j, and take the N^{th} equation to be

$$\sum_{j=1}^{N} X_j = 1.$$

The system of Equations (7) and (7a) can be solved with better success than (2). Using more data points gives some improvement but a serious limitation is that the matrix

$$A_{jJ} \equiv \sum_{i=1}^{M} B_{ij} B_{iJ} \qquad (8)$$

with the specification (7a) is nearly singular.

Thus, if as a practical matter we are limited to four significant figures in the determination of λj and $P(t_i)$, then with (7a) trial calculations show that we are limited to analyzing mixtures of three gases with widely separated characteristic λj's. This is equivalent to demanding widely spaced molecular weights because we have seen that the time constant is linear with the square root of molecular weight.

5.2 Obtaining a More Favorable System of Equations to Solve for the Composition of a Gas Mixture

To obtain a more favorable matrix A_{jJ} (i.e., larger determinant) the response (7a) can be changed. A direct way of accomplishing this is to use two membranes to obtain a peaked response which would produce better definition of the solutions X_j.

A possible method of obtaining a peaked reponse is shown in Figure 15 with its electric circuit analog below. With boundary conditions $q_1(0) = q_0$ and $q_2(0) = 0$ and $R_1 = R_2 = R$ and $C_1 = C_2 = C$ the solution (for the electric circuit) is

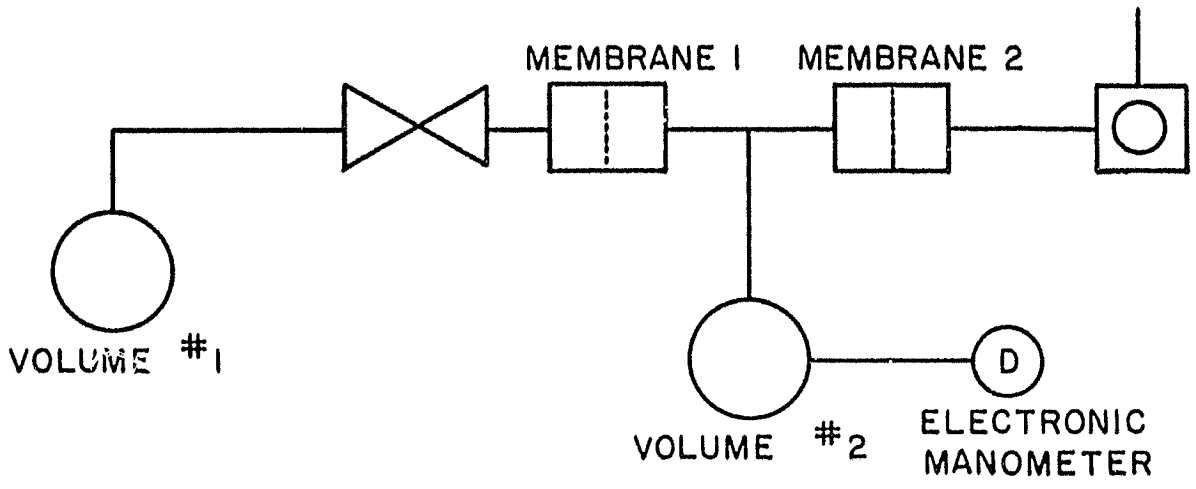

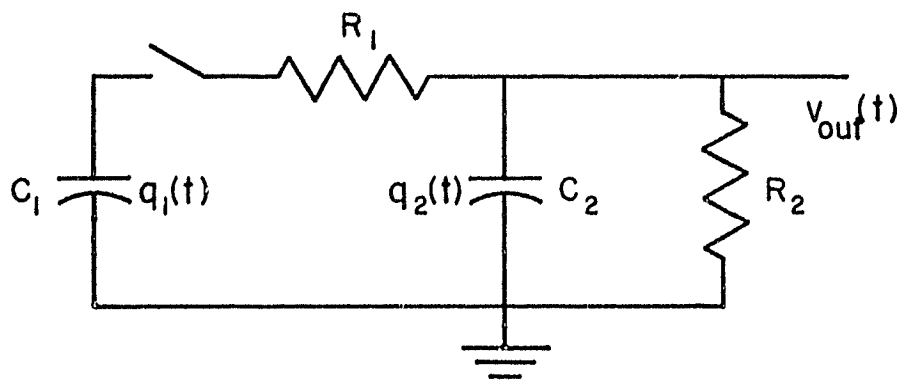

FIGURE 15 VACUUM SYSTEM AND ELECTRICAL ANALOG TO PRODUCE A PEAKED RESPONSE

$$q_2(t) = \frac{2q_0}{\sqrt{5}} \exp\left(-\frac{3t}{2RC}\right)\sinh\left(\frac{\sqrt{5}\,t}{2RC}\right)$$

with the time to peak given by

$$T_p = 0.86RC.$$

If, in the vacuum system of Figure 15, $V_1 = V_2 = V$, $F_{1j} = F_{2j} = F_j$, $P_1(0) = P_0$, $P_2(0) = 0$, then using the discussion of Section 2.1 regarding the electrical-vacuum analogy, we see that Equation (7) may be used with

$$B_{ij} = \frac{2P_0}{\sqrt{5}} \exp\left(-\frac{3t_i F_j}{2V}\right)\sinh\left(\frac{\sqrt{5}\,t_i F_j}{2V}\right) \qquad (7b)$$

to determine the X_j for a gas mixture undergoing molecular flow. As shown by actual calculations, the waveform (7b) used in Equation (7) gives better-defined solutions for the X_j than if waveform (7a) is used.

Figure 16 and Figure 17 show response curves of the form (7b) computed for a typical system of two membranes as in Figure 15. The curves marked "SUM" are sums of the curves for the gases present in the mixture. The peaks of both "SUM" curves are at about seventeen seconds, and the peak values are only about four percent apart even though the compositions are drastically different. We would expect some difficulty, therefore, in determining the compositions of the two mixtures, even assuming prior knowledge of the species of the four gases actually present.

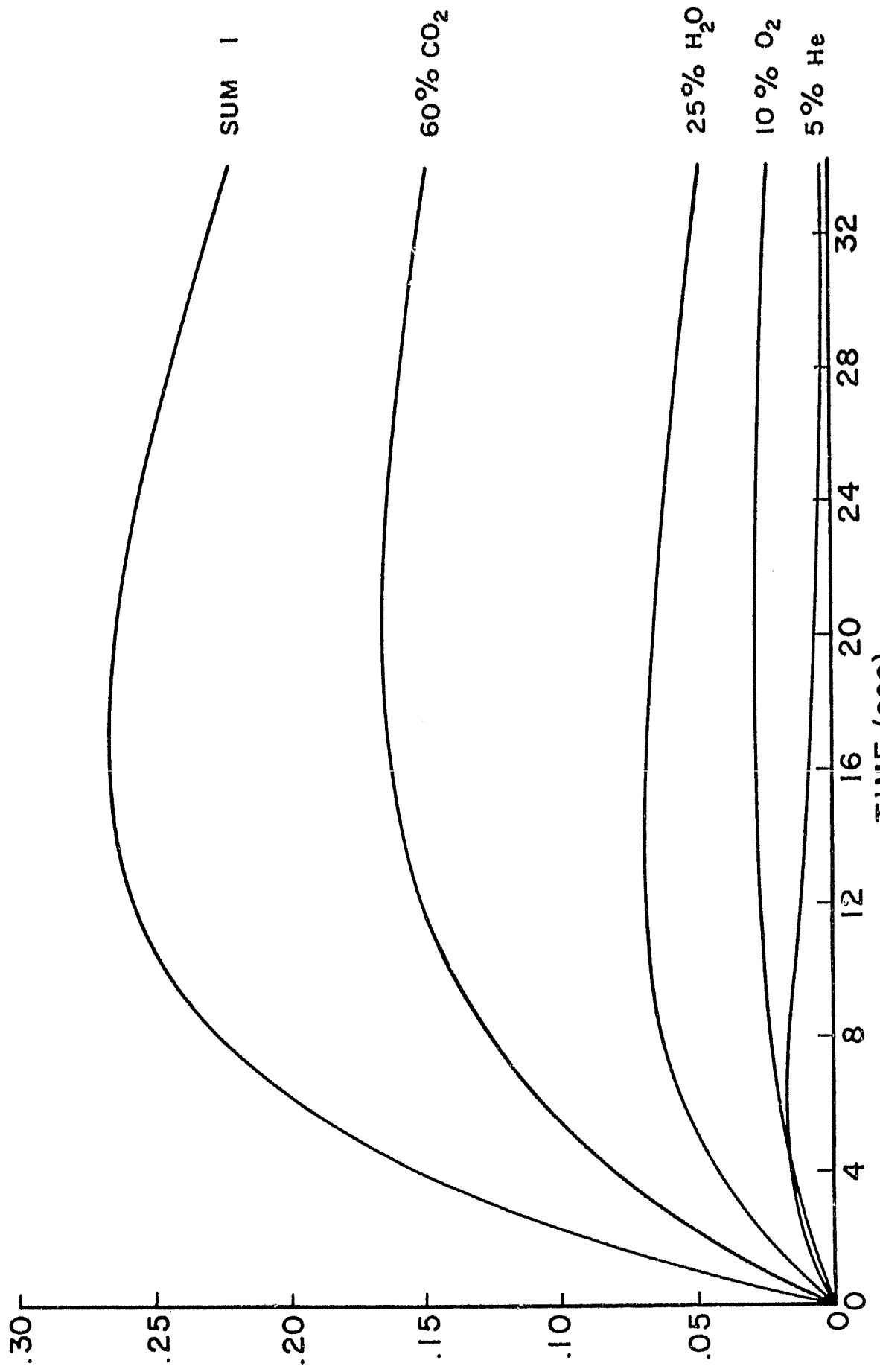

FIGURE 16 CALCULATED RESPONSE CURVES FOR A FOUR-GAS MIXTURE, WIDELY SPACED MOLECULAR WEIGHTS, IN THE SYSTEM OF FIGURE 15

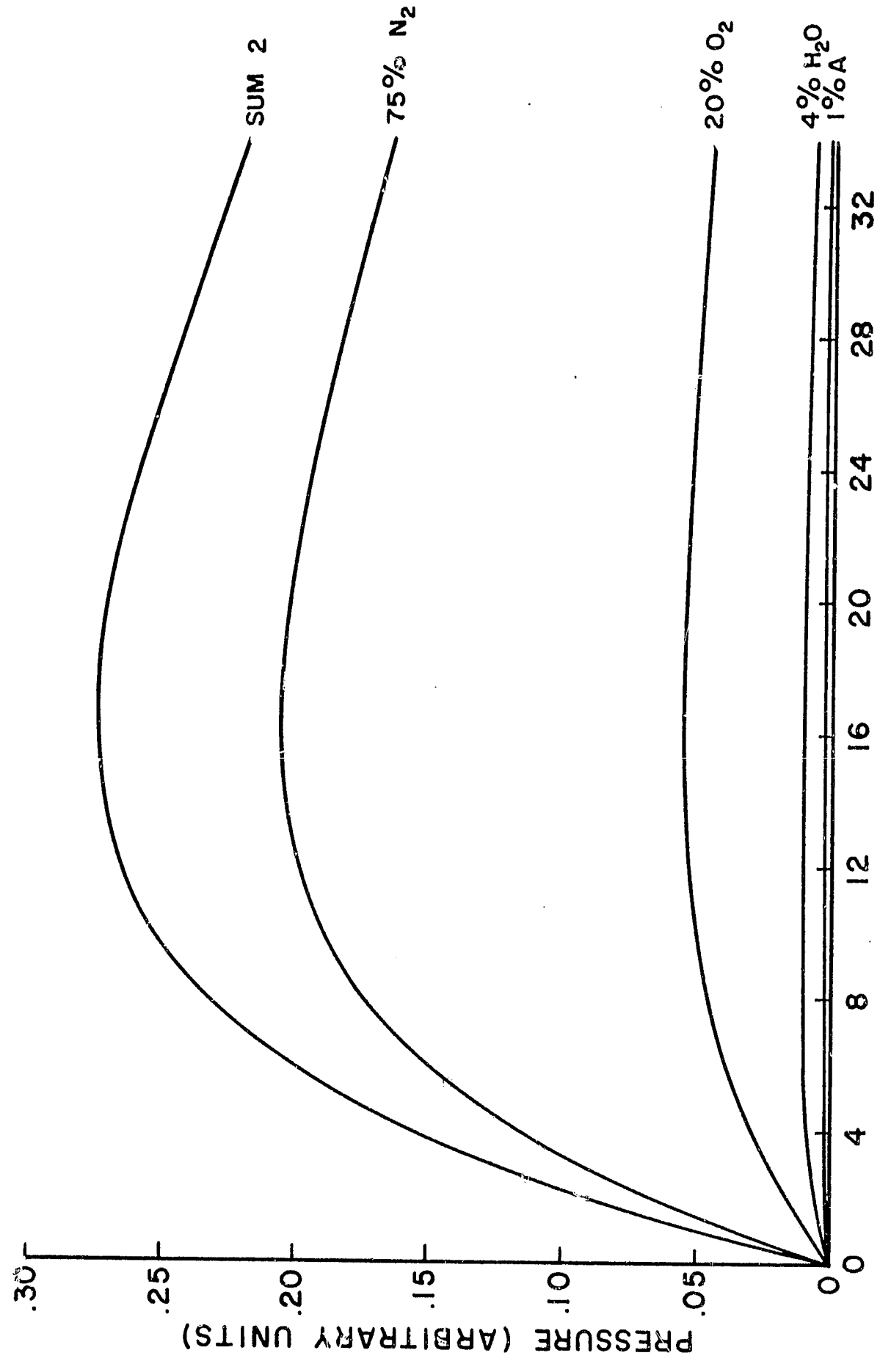

FIGURE 17 CALCULATED RESPONSE CURVES FOR FOUR-GAS MIXTURE, TWO NARROWLY SPACED MOLECULAR WEIGHTS (N_2 AND O_2) IN THE SYSTEM OF FIGURE 15

For times greater than twice the time to peak, the "SUM" curves in Figures 16 and 17 have long, slowly decreasing tails which are not shown here. However, it turns out that the shape of the tails is just as important as the early part of the curve in the determination of the solutions to Equations (7). The practical limit on the length of the tail that was used here is that point at which the percentage measurement error became three times the percentage error near the peak. Obviously, other criteria could be used.

5.3 Solution of the System of Linear Equations for the Composition of a Gas Mixture

The system of linear Equations (7) is of the same form no matter what vacuum system were to be used for analysis of a gas mixture. The response B_{ij} is changed from system to system but it is always made up of sums and products of exponentials. Therefore most considerations applying to the solution of (7) with the particular waveform (7b) will apply to data analysis for any "RC" vacuum system.

The system (7) may be written as

$$AX = D, \tag{9}$$

$$D \equiv \sum_{i=1}^{M} P(t_i)\, B_{iJ} \tag{9a}$$

and A was defined by Equation (8). Note that A, which is square, depends only upon the time constants of the gases present and the times at which the data curve is taken, but not upon the values $P(t_i)$. The vector D is, however, determined by all these quantities.

The solution of (9) is difficult when A is derived from exponentials because A is often nearly singular. Most direct linear

equation solving methods are not successful when A is nearly singular. Therefore the solution of (9) will be divided into two parts: (1) the inversion of A and (2) the calculation of physically acceptable solutions for X. If A is nearly singular, some elements of A^{-1} may be three to six orders of magnitude larger than the elements of A, but these inverses can still be used successfully if enough significant digits are retained.

A standard computer matrix inversion routine may be used to get an approximate inverse A_1^{-1}. Then an iteration can be developed as follows to add digits. Define R and A_R:

$$AA_1^{-1} \equiv I - R,$$

$$A(A_1^{-1} + A_R) \equiv I.$$

Substituting

$$I - R + AA_R = I,$$

$$AA_R = R.$$

Then approximate A_R

$$A_R \simeq A_1^{-1} R.$$

Define

$$A_2^{-1} \equiv A_1^{-1} + A_R = A_1^{-1} (I + R)$$

and since

$$R = I - AA_1^{-1},$$

$$A_2^{-1} = A_1^{-1} (2I - AA_1^{-1}).$$

This may be extended to

$$A_{j+1}^{-1} = A_j^{-1} (2I - AA_j^{-1}) \qquad (10)$$

which converges if the norm of R, N(R) < 1 where

$$\left[N(R)\right]^2 \equiv \sum_{ij} R_{ij}^2$$

Bodewig (1959) shows (10) derived by a different method.

The iteration (10) is cut off when enough digits have been developed in A_j^{-1} so that the off-diagonal terms of AA_j^{-1} are a few orders of magnitude smaller than the elements of A. If iteration (10) will not converge, then taking the data points $P(t_i)$ at greater time intervals will give a more nonsingular A. In fact best results will be obtained if the fewest possible points $P(t_i)$ are used, consistent with the averaging advantage to be obtained from the least-squares approach, with the points taken at wide intervals. A good compromise between the aim of obtaining a nonsingular A (by using few data points widely spaced), and the statistical advantage of averaging a large number of data points has been found to be 10 to 20 data points.

5.4 Accuracy of Solutions for Gas Mixture Compositions

The accuracy of solutions to the system (9) with exponential and exponential-like waveforms is extremely sensitive to the number of significant digits used. Furthermore, best results are obtained if the vector D has at least one more digit than A.

One method of obtaining four or five place accuracy in the measurement of the pressure waveform would be to generate a known waveform and measure the differences of the unknown waveform from it. Thus in Figure 18 if the values of the known curve were calculated at each time to within 0.1%, and if the unknown curve B differed from A by only 10 to 100 mv out of, say 10 volts, then the values of B could be determined to about 0.1%. This would be the limit of accuracy of most pressure transducers now available.

5.5 Improving the Accuracy of Solutions for Gas Mixture Compositions

Suppose that four digits can be measured for A and D of the system (9). The solution vectors X_j may still vary drastically for small changes in D. However, the boundary conditions are still to be imposed that for an acceptable solution vector all X_j must be between zero and one. For the response (7b) one column of A^{-1} is usually larger than all the others, so the one D_j corresponding to that column may be swept over the range of uncertainty in $P(t_i)$. Then all the solutions, both physical and non-physical can be obtained, and a range of possible values for the X_j will be determined.

Consider the following example in which D_3 is varied from 0.96070 to 0.96089 in increments of 0.00001.

$$\begin{bmatrix} .5677 & .6737 & .6645 & .6478 \\ .6737 & .9210 & .9474 & .9425 \\ .6645 & .9474 & .9863 & .9869 \\ 1.0 & 1.0 & 1.0 & 1.0 \end{bmatrix} \begin{bmatrix} X_1 \\ X_2 \\ X_3 \\ X_4 \end{bmatrix} =$$

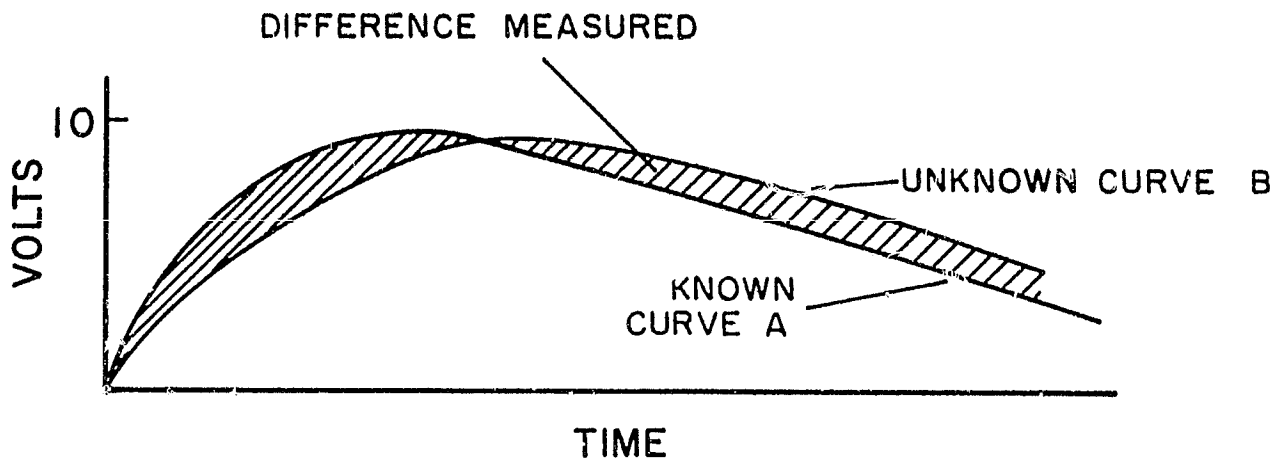

FIGURE 18 DETERMINATION OF AN UNKNOWN CURVE B BY MEASURING THE (SMALL) DIFFERENCE BETWEEN B AND A KNOWN CURVE A

$$\begin{bmatrix} .6520 \\ .9242 \\ .96070, \quad .96071 \quad \text{to} \quad .96089 \\ 1.0 \end{bmatrix}.$$

All of the solution vectors for X except the ".96080" vector have at least one X_j negative. The ".96080" vector is shown in Figure 19 along with the two adjacent solutions. The solutions not shown vary even more widely.

Note, however, that the three points where the vectors "cross" are quite well defined. The minimum value for H_2O or O_2 (or any of the gases!) is zero, so we can use the zeros of H_2O and O_2 together with the "crossover" points to determine the uncertainties in composition of the mixture as shown by the shaded areas. This is simply an interpolation between the three vectors ".96079, .96080, .96081." This interpolation can be performed whether or not any vectors whatsoever were actually calculated that are physically acceptable, as long as the "crossovers" are defined. It is only a coincidence here that the correct solution shown by the dotted line is close to the ".96080" vector.

Figure 20 shows solutions for a mixture of four gases. The solid lines, again, show three solutions found by "sweeping" D and none of them are physical, though they are the closest solutions found. Interpolation as described above gives the shaded uncertainty region which is tighter than in Figure 19, even though the molecular weights of N_2 and O_2 are closer in this example than the molecular weights of any two gases in Figure 19. The reason is that H_2O and A are such small constituents.

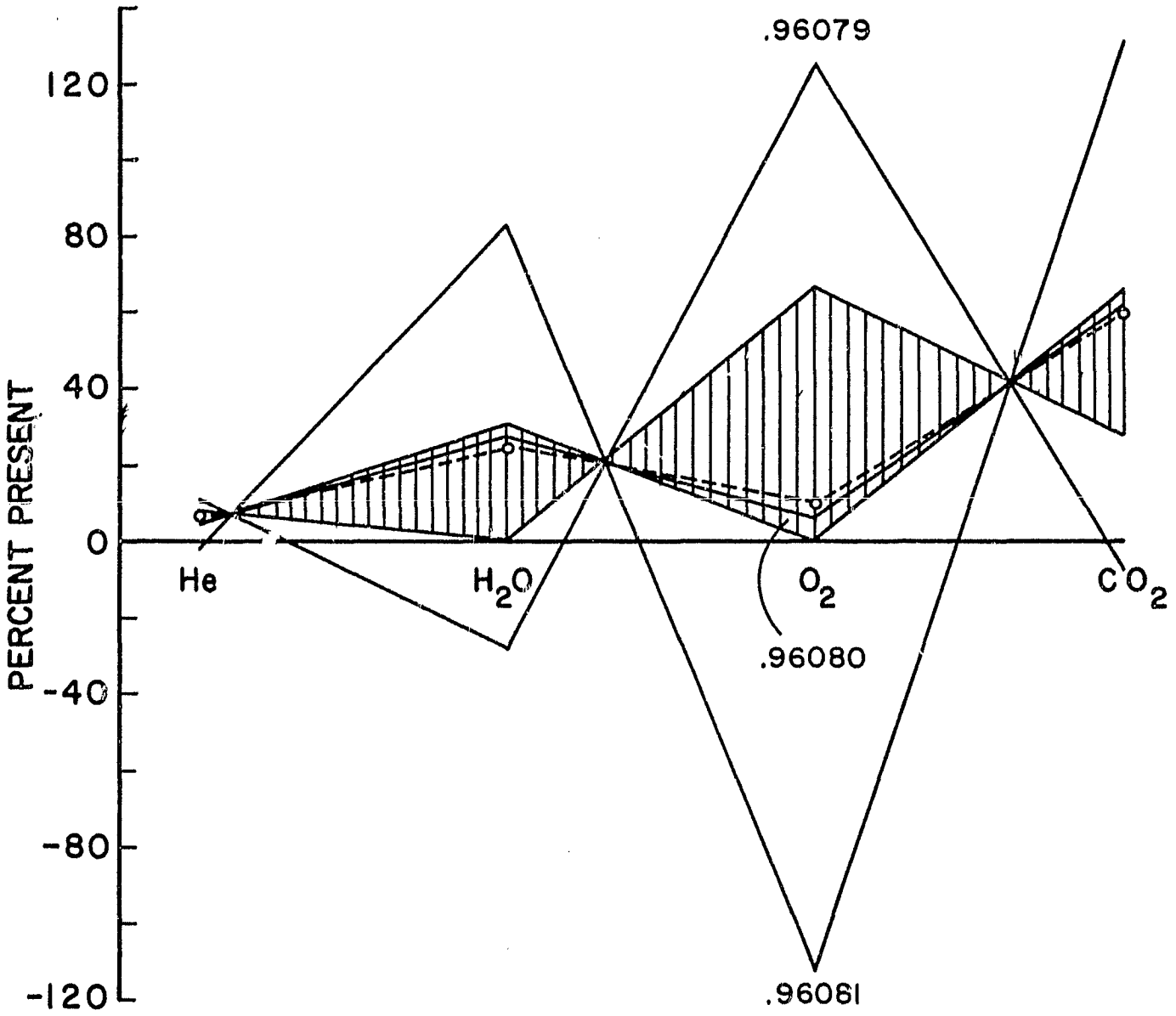

FIGURE 19 FOUR GAS MIXTURE WITH WIDELY SPACED MOLECULAR WEIGHTS, THREE SOLUTIONS. CORRECT SOLUTION AND UNCERTAINTIES ARE SHOWN

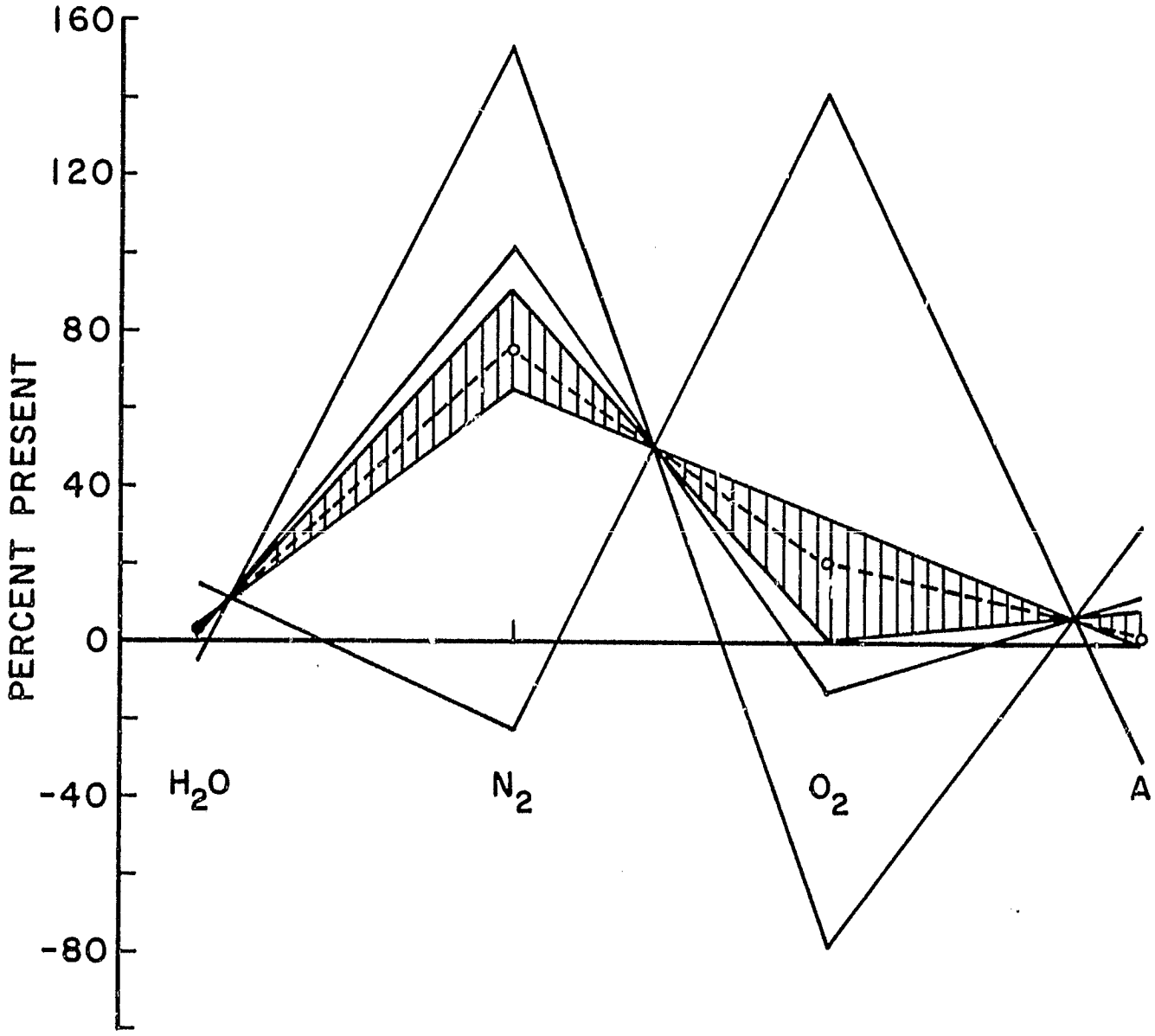

FIGURE 20 FOUR GAS MIXTURE WITH TWO NARROWLY SPACED MOLECULAR WEIGHTS (N_2 AND O_2). THREE SOLUTIONS, CORRECT SOLUTION AND UNCERTAINTIES ARE SHOWN

Mixtures having one or more small percentage components are analyzed with less error than more evenly divided mixtures because the presence of small percentage components can produce negative solutions more quickly. With the waveform (7b) one always gets negative solutions before getting solutions greater than one. This is because of the asymmetry around zero of the boundary condition $0 < X_j < 1$.

Figures 21 and 22 show solutions for three-gas mixtures which are physical over the whole range of "sweep" in D, though Figure 22 shows solutions that are just about to go negative. Unlike Figures 19 and 20 which show only three of the closest solutions, Figures 21 and 22 show the range of all twenty-one solutions for twenty-one column vectors D, with D_2 taken over the range of $\pm 10^{-5}$ (at intervals of 10^{-6}). Therefore the solutions for these three-gas mixtures are much more stable than for these four-gas mixtures.

Figure 23 shows an analysis using only three digits in D with four digits in A. The solutions are very unstable, and the correct solution falls outside the calculated uncertainty limits.

5.6 Optimization of the Vacuum System for Data Analysis

Greatly more complicated vacuum systems than the one shown in Figure 15 are possible, utilizing multiple volumes and several membranes to produce more than one peak in the response B_{ij}. These multiple-peaked responses will always be sums and differences of exponentials. These responses have closely spaced peaks, even for pure gases with widely separated molecular weights; and the waveforms have slowly decaying tails which prevent the peak from being very sharp.

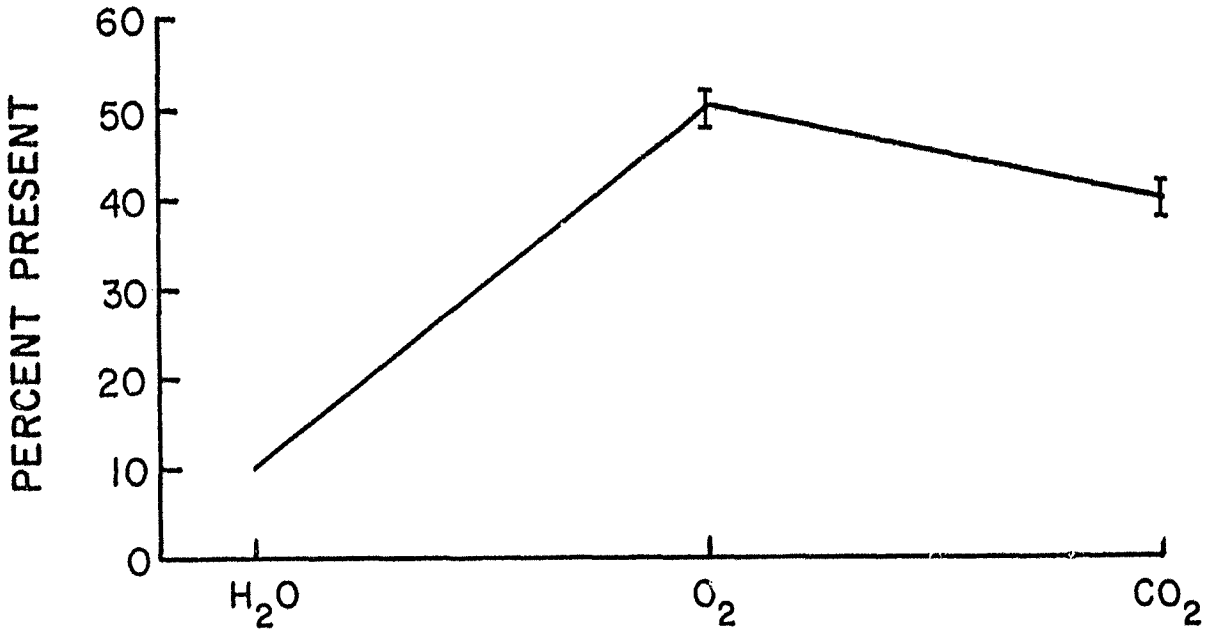

FIGURE 21 THREE GAS MIXTURE WITH WIDELY SPACED MOLECULAR WEIGHTS

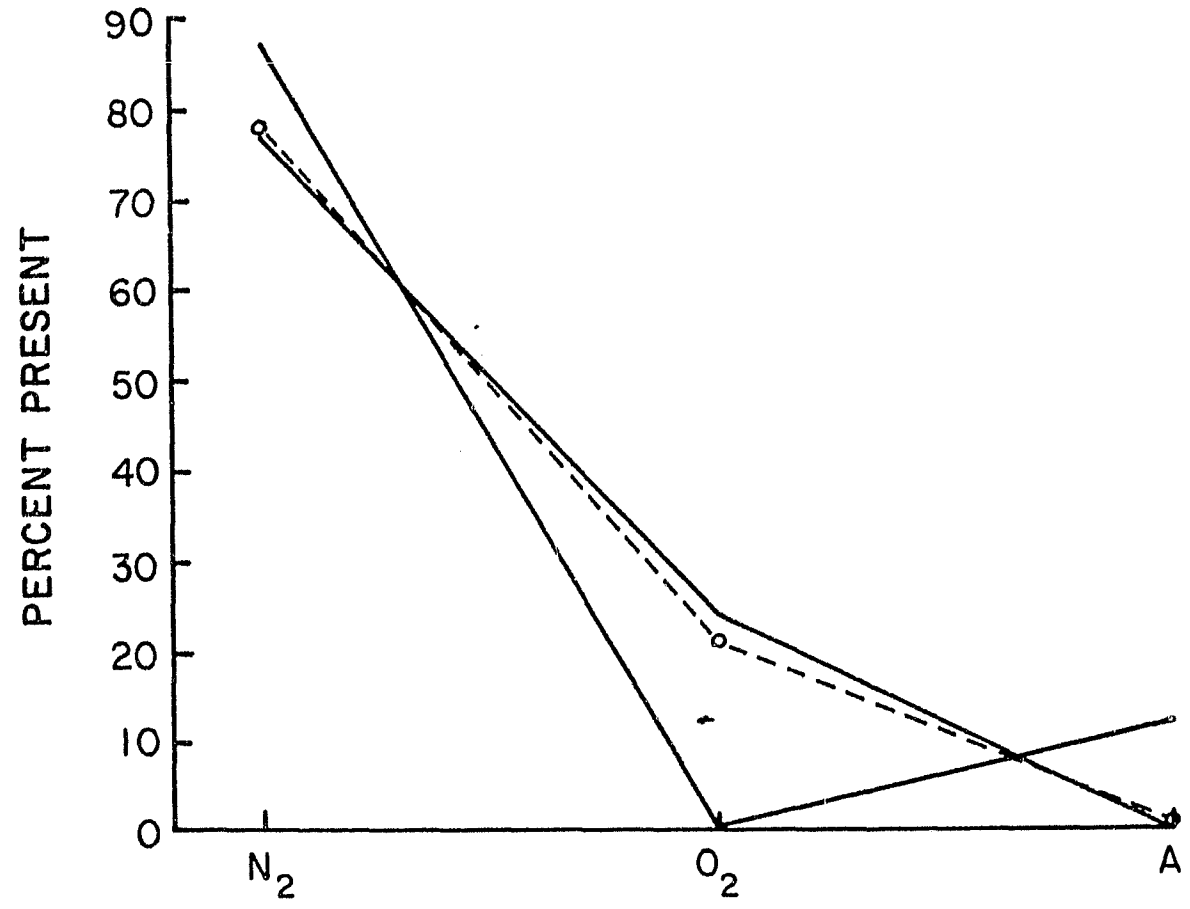

FIGURE 22 THREE GAS MIXTURE WITH TWO NARROWLY SPACED MOLECULAR WEIGHTS (N_2 AND O_2). CORRECT SOLUTION AND UNCERTAINTIES ARE SHOWN

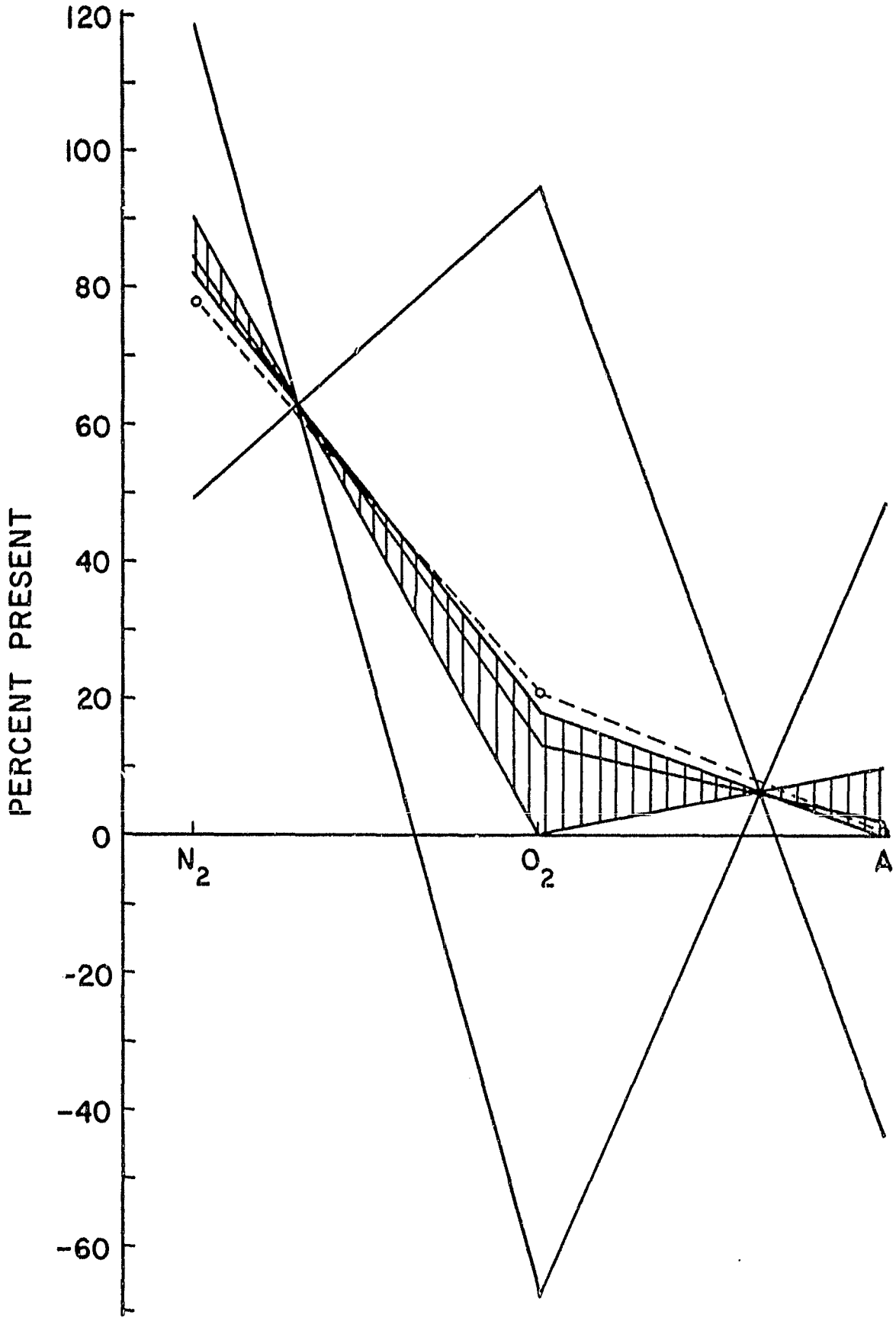

FIGURE 23 THREE GAS MIXTURE AS IN FIGURE 20 BUT WITH ONLY THREE DIGITS. ANALYSIS INCORRECT

To produce better-defined peaks in the response of such a system it is necessary to choose the values of the volumes and membrane conductances to separate the peaks for various pure gases and bring down the tails as much as possible. The optimization of these two effects usually requires the sacrifice of some peak height.

The sharpening of the response of Figure 16 will now be discussed, and the procedure is similar for the analysis of any multiple-membraned system.

In the system of Figure 15 let

$$R_2 = \frac{R_1}{\alpha} \quad , \quad C_2 = \frac{C_1}{\beta} \quad , \quad R_1 C_1 = \frac{1}{a}$$

where now α and β are the unknowns to be determined for the sharpest peaks. The solution with boundary conditions $q_1(0) = q_0$, $q_2(0) = 0$ is

$$q_2(t) = \frac{q_0}{c} \; e^{-abt} \sinh act \qquad (11)$$

where

$$b = \frac{1}{2}(1 + \beta + \alpha\beta) \qquad (11a)$$

and

$$c^2 = b^2 - \alpha\beta \quad . \qquad (11b)$$

Taking the size difference in C_1 and C_2 into account we have

$$V_{out}(t) = \frac{1}{C_2} \; q_2(t) = \frac{\beta}{C_1} \; q_2(t) \quad .$$

The time to peak of (11) is

$$T_p = \frac{1}{2ac} \ln\left(\frac{b + c}{b - c}\right)$$

and at large t the response (11) drops off as

$$e^{-a(b - c)t} .$$

Therefore we will try to obtain the greatest distance between peaks with the fastest drop of the tail by maximizing the product

$$K \equiv \frac{b - c}{2c} \ln\left(\frac{b + c}{b - c}\right) . \qquad (12)$$

Functions other than the direct product could be considered, of course, but (12) was chosen for simplicity.

Now for a maximum

$$\frac{\partial K}{\partial b} = 0 = -\frac{2c}{b + c} + \ln\left(\frac{b + c}{b - c}\right) \qquad (13a)$$

and

$$\frac{\partial K}{\partial c} = 0 = \frac{2b}{b + c} - \ln\left(\frac{b + c}{b - c}\right) - \frac{b - c}{c} \ln\left(\frac{b + c}{b - c}\right) ,$$

$$0 = \frac{2b}{b + c} - \frac{2b}{b + c} - \frac{2bc}{(b + c)^2} - \frac{8bc^2}{(b + c)^3} - \ldots . \qquad (13b)$$

The last line is obtained from the identity

$$\ln(z) = \frac{z - 1}{z} + \frac{1}{2}\left(\frac{z - 1}{z}\right)^2 + \frac{1}{3}\left(\frac{z - 1}{z}\right)^3 + \ldots, \; z > \frac{1}{2} .$$

It is clear that Equations (13a) and (13b) will only be satisfied in the limits as $b \to \infty$ and $c \to 0$. The statements (11a) and (11b) do not, however, allow this limit, so we shall have to find

α and β which produce a large ratio b/c.

Figure 24a shows K as a function of α and β and it is clear that K increases for large α and small β. The ratio b/c has reached 10 for the pair $\alpha = 100 = \frac{1}{\beta}$ from about b/c = 1.3 for $\alpha = 1 = \beta$. For $\alpha \geq 2$ the greatest K is obtained for β such that $\alpha\beta = 1$.

The quantity $P(\alpha, \beta)$ in Figure 24b gives an indication of the relative peak heights. P is only an approximate indication, though, because the peak times vary from $T_p = 0.86R_1 C_1$ at $\alpha = 1 = \beta$ to $T_p = 1.00R_1 C_1$ at $\alpha = 100 = \frac{1}{\beta}$.

The following figures show the importance of making the best choice of volume sizes and conductances to produce the most clearly defined waveforms. In the simple case of Figure 15 this means choose α as large as possible and β as small as possible, though there is little improvement for $\alpha > 100$ or $\beta < 0.01$. Also choose $\alpha\beta = 1$. The choice of $\alpha = 100 = \frac{1}{\beta}$ causes about an order of magnitude decrease in peak height, but this would not usually be a serious problem.

In a comparison of the previous solutions when $\alpha = \beta = 1$ (K = 0.32) with the case when $\alpha = 100 = \frac{1}{\beta}$ (K = 0.90), it is immediately apparent that the solutions to the latter case are much more stable than the solutions to the former. In Figure 25, 13 physical solutions were found (using the same sweep range and interval) compared with only one physical solution found in Figure 19 where $\alpha = \beta = 1$. The most important fact is that the improved choice of system parameters gives smaller uncertainties in the results as shown by Figures 25 to 28 as compared with Figures 19 to 22.

$$K(\alpha, \beta) = \frac{b - c}{2c} \ln \frac{b + c}{b - c}$$

α =	β = .01	.02	.05	0.1	0.2	0.5	1.0
0.1				.03			.09
0.5							.25
1.0	.04			.21		.36	.33
2.0					.45	.46	.37
5.0				.43	.62	.44	.31
10	.25		.63	.72	.58	.35	.22
20		.44	.79	.63			.15
50	.68	.87	.49	.39			
100	.90	.68	.40	.25			

(A)

$$P(\alpha, \beta) = \frac{\beta}{c}$$

α =	β = .01	.02	.05	0.1	0.2	0.5	1.0
0.1				.02			1.0
0.5							.97
1.0	.01			.20		.70	.90
2.0					.41	.67	.88
5.0				.27	.43	.41	.37
10	.02		.16	.31	.27	.21	.20
20		.05	.21	.16			.10
50	.04	.14	.06	.04			
100	.10	.04	.03	.02			

(B)

FIGURE 24 (A) PEAK SHARPNESS K WHERE INCREASING K INDICATES SHARPER PEAKS
(B) APPROXIMATE RELATIVE PEAK HEIGHTS, P

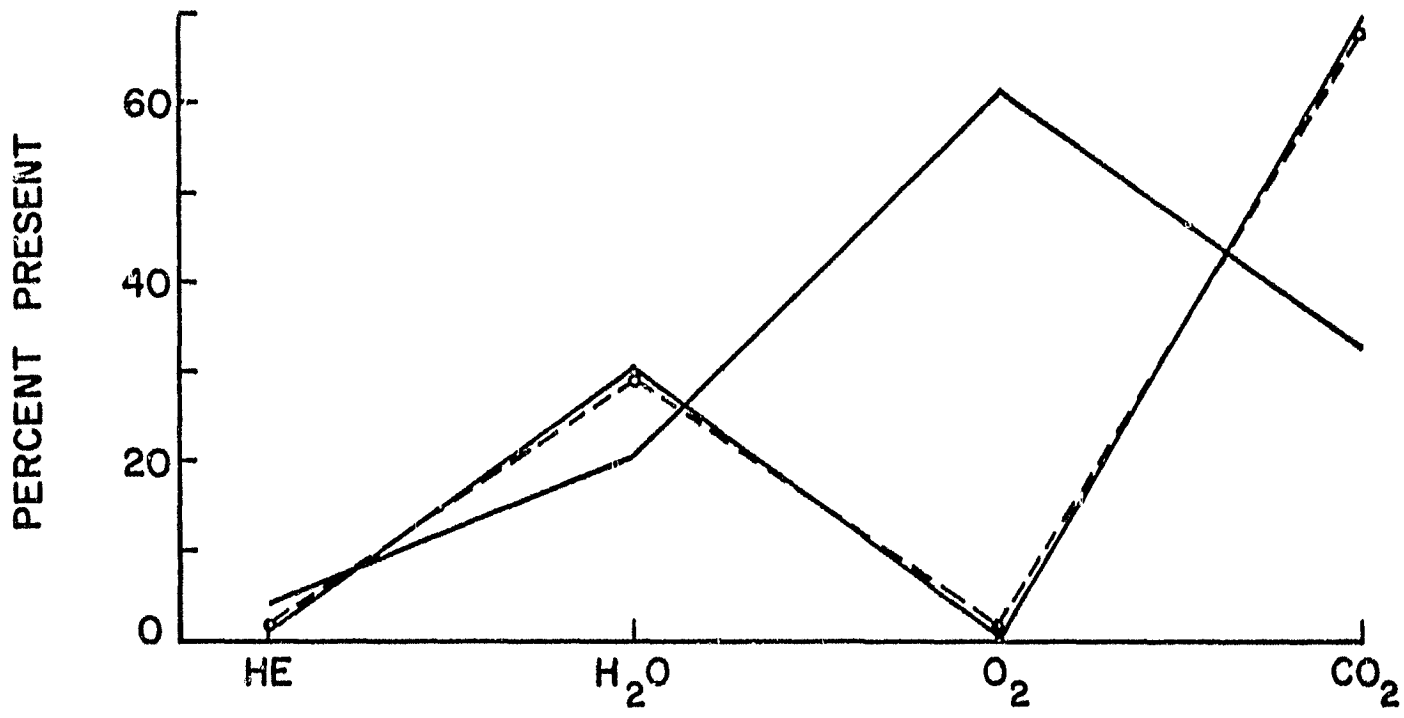

FIGURE 25 FOUR GAS MIXTURE SIMILAR TO THAT OF FIGURE 19, BUT WITH $\alpha = 100 = \frac{1}{\beta}$ THIRTEEN PHYSICAL SOLUTIONS WERE GENERATED BETWEEN THESE BOUNDARIES FOR THE SAME TYPE OF SWEEP THAT GENERATED ONE SOLUTION IN FIGURE 19

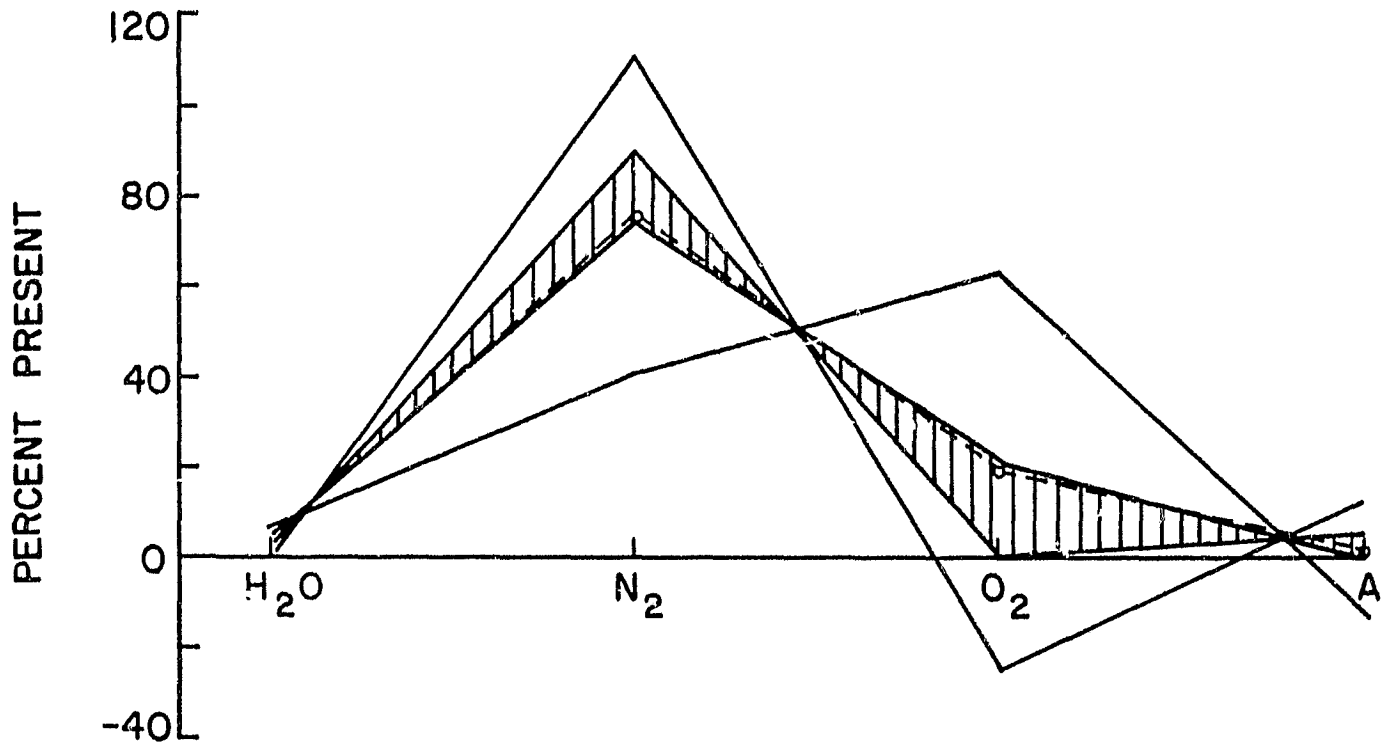

FIGURE 26 FOUR GAS MIXTURE SIMILAR TO THAT OF FIGURE 20, BUT $\alpha = 100 = \frac{1}{\beta}$ GIVES SMALLER REGIONS OF UNCERTAINTY

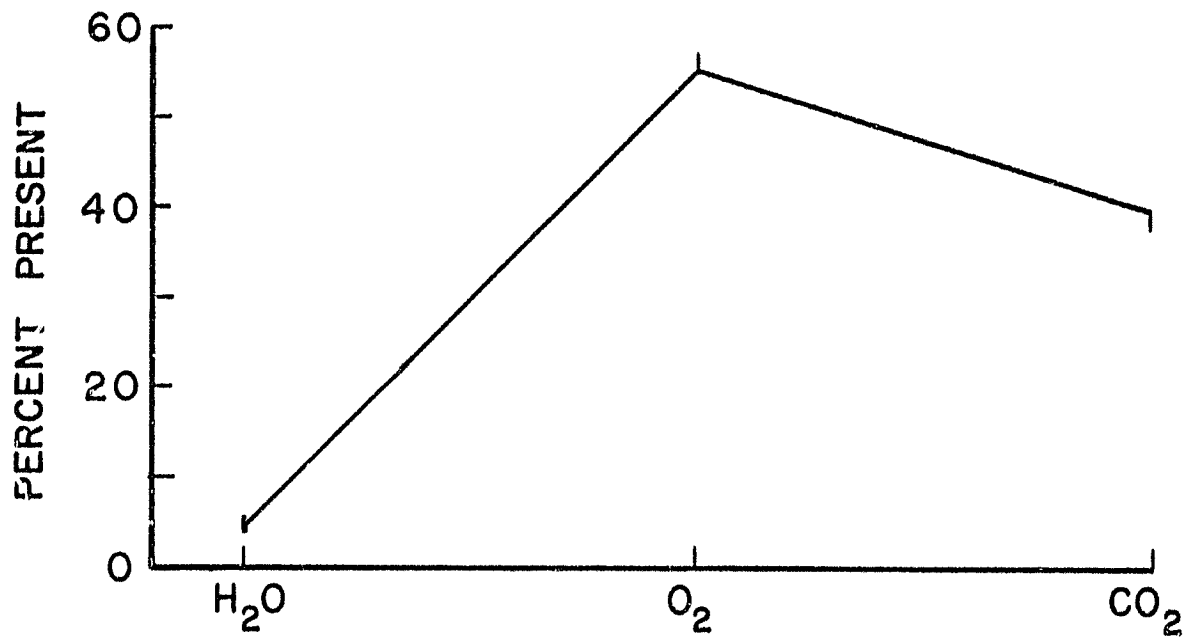

FIGURE 27 THREE GAS MIXTURE SIMILAR TO FIGURE 21, BUT $\alpha = 100 = \frac{1}{\beta}$ GIVES SMALLER UNCERTAINTIES

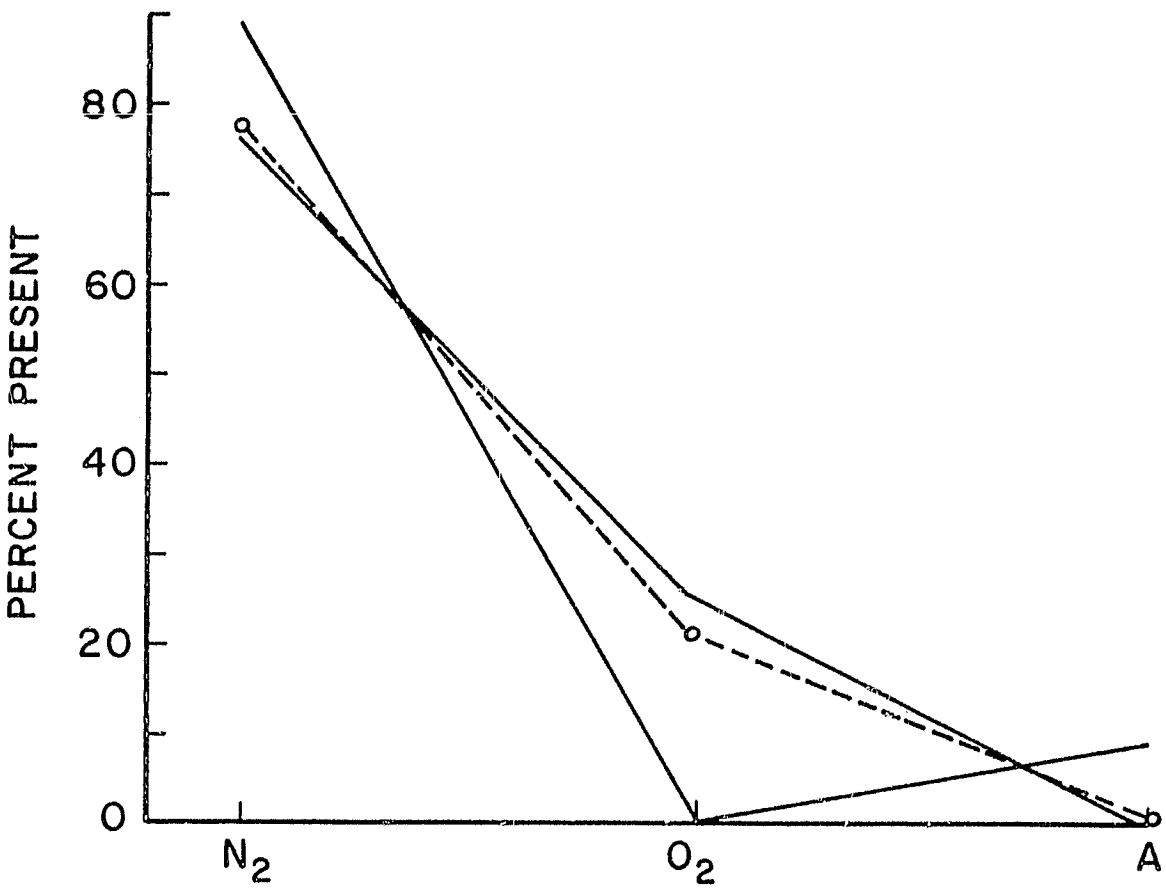

FIGURE 28 THREE GAS MIXTURE SIMILAR TO FIGURE 22, BUT $\alpha = 100 = \frac{1}{\beta}$ GIVES SMALLER UNCERTAINTY FOR ARGON

Figure 29 shows the correct analysis of a five gas mixture (albeit with a large uncertainty) by the system with $\alpha = 100 = \frac{1}{\beta}$. All attempts to analyze five gases with $\alpha = \beta = 1$ failed. The analysis of five gases with more closely spaced molecular weights failed in Figure 30 because the correct solution vector does not lie within the region of uncertainty, nor does it intersect the crossover points.

Figure 31 shows greater error than the two previous solutions for this mixture caused by choosing $\alpha = 20$, $\beta = 1$ where K is only 0.1. Figure 32 shows the inability of this system (K = 0.1) to analyze this four gas mixture (because the correct solution vector does not intersect the crossovers) which was analyzed correctly by both the previous systems.

5.7 Computer Program to Calculate Gas Mixture Compositions

Figure 33 is a flow chart for the computer program to calculate $X = A^{-1}D$. Figures 34a and 34b are the listing of the actual computer program.

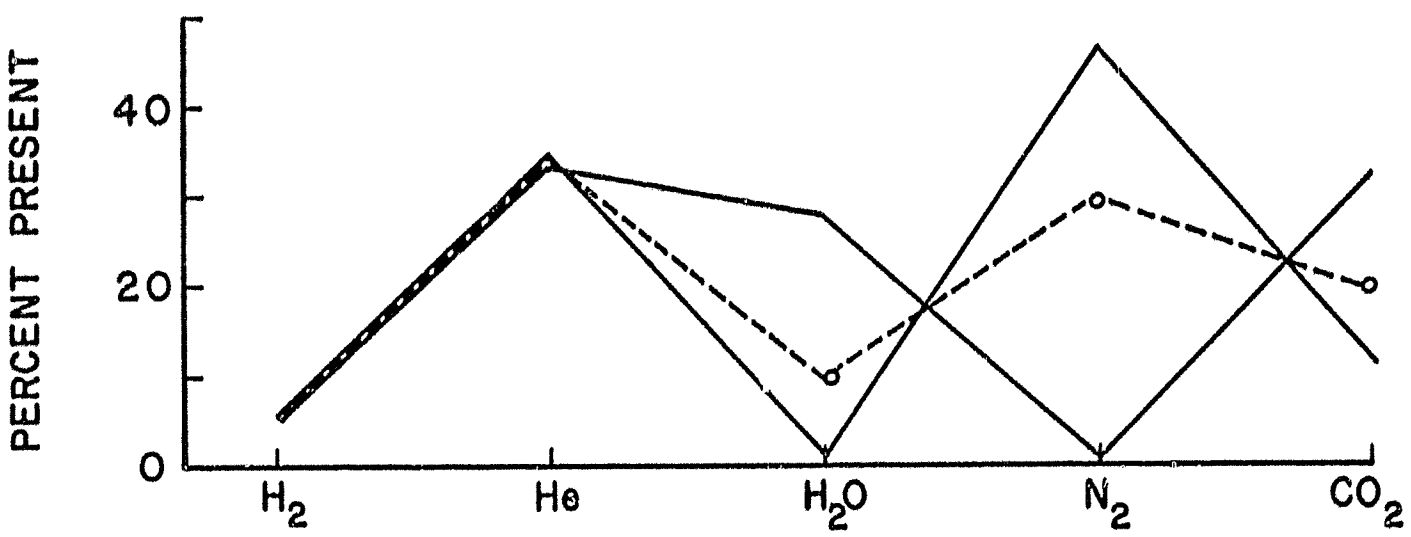

FIGURE 29 FIVE GAS MIXTURE WITH $\alpha = 100 = \frac{1}{\beta}$ WAS ANALYZED INCORRECTLY BY THE SYSTEM HAVING $\alpha = \beta = 1$

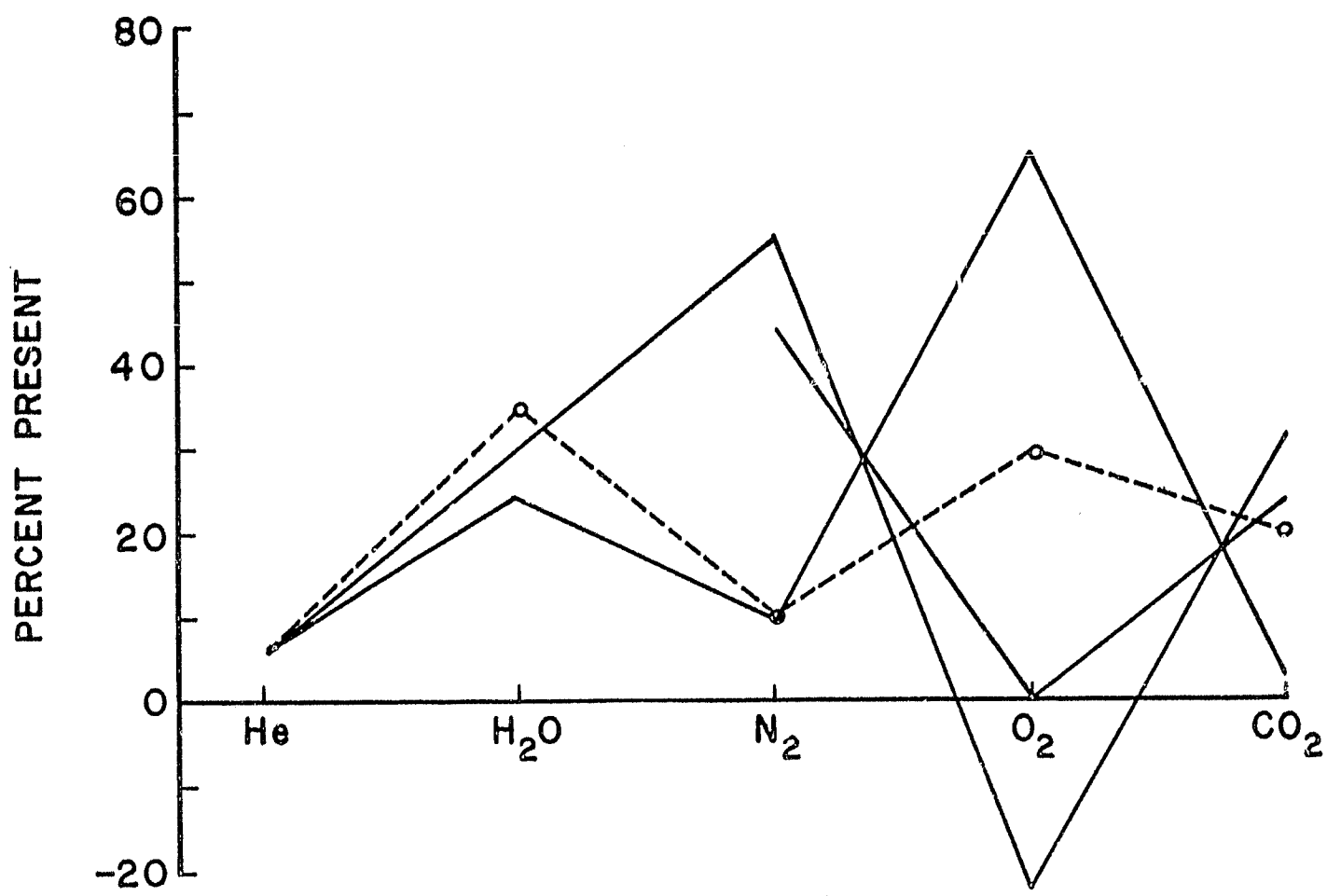

FIGURE 30 FIVE GAS MIXTURE WITH $\alpha = 100 = \frac{1}{\beta}$ AND MORE CLOSELY SPACED MOLECULAR WEIGHTS. INCORRECT

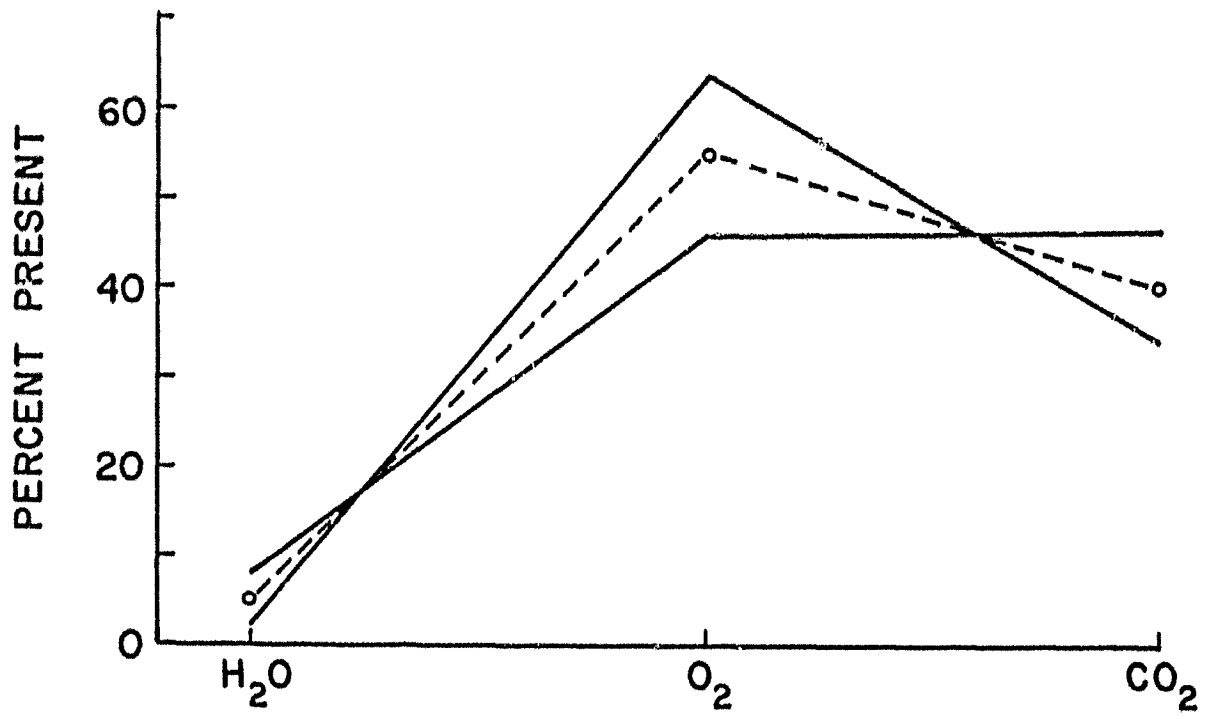

FIGURE 31 THREE GAS MIXTURE WITH $\alpha = 20$, $\beta = 1$ SHOWS MORE UNCERTAINTY THAN THE TWO PREVIOUS SOLUTIONS

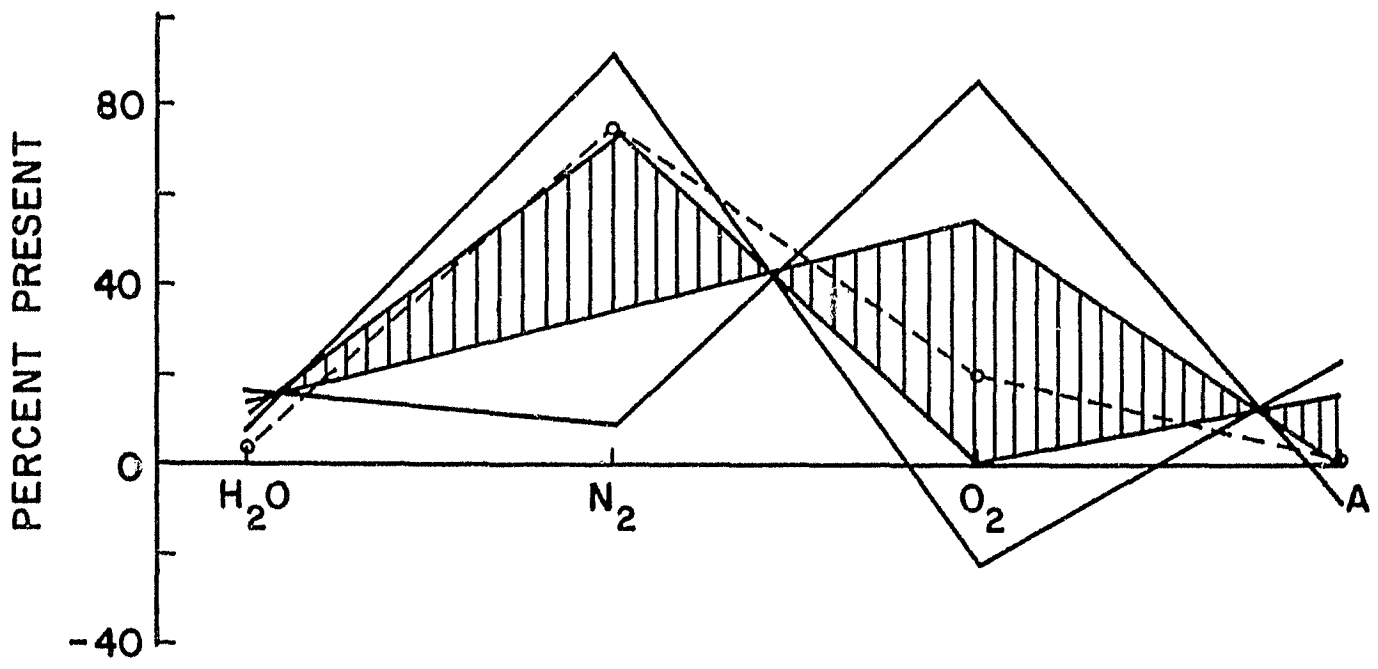

FIGURE 32 FOUR GAS MIXTURE WITH $\alpha = 20$, $\beta = 1$. ANALYZED INCORRECTLY

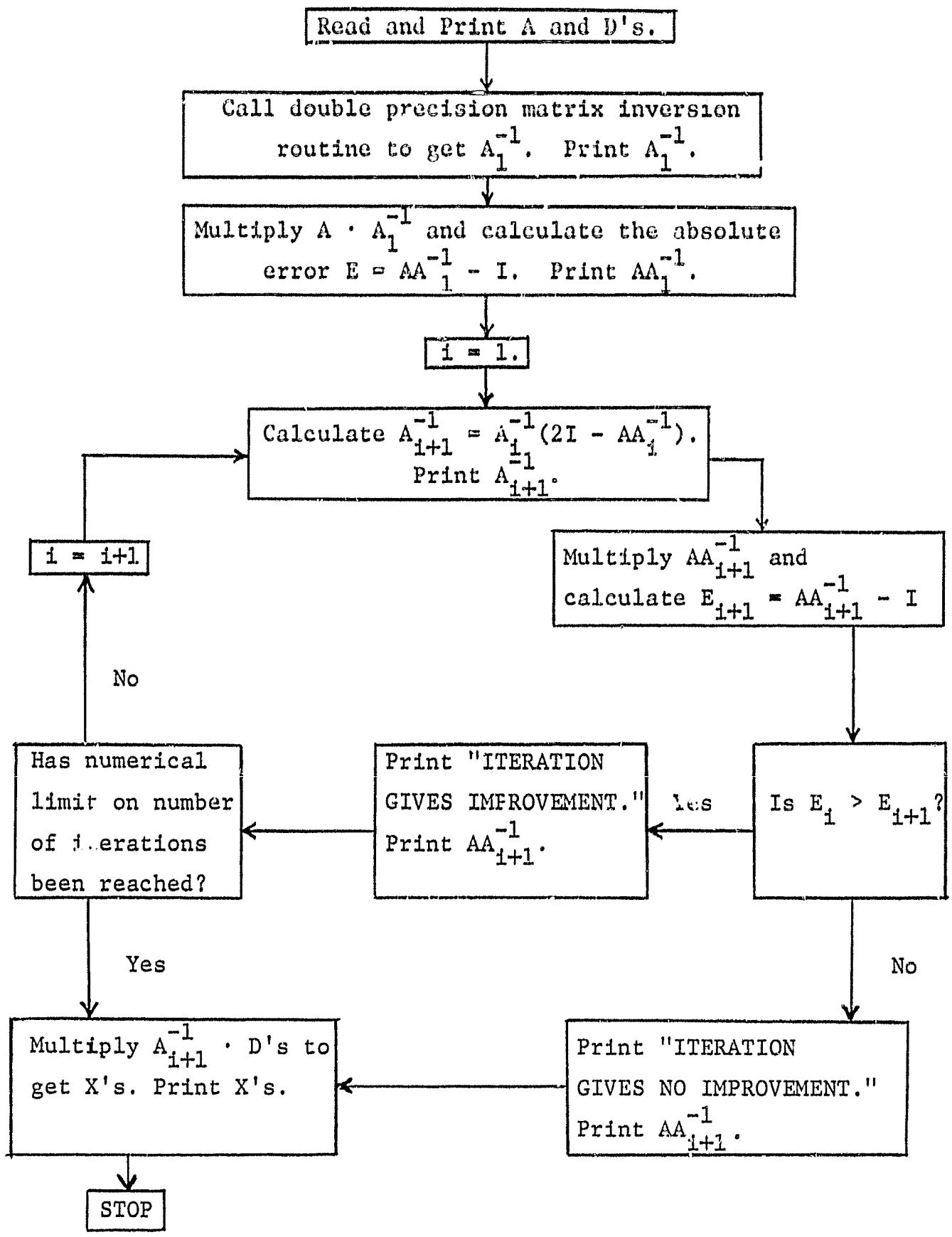

FIGURE 33 FLOW CHART FOR A PROGRAM TO SOLVE AX = D BY $X = A^{-1} D$ USING $A_{i+1}^{-1} = A_i^{-1}(2I - AA_i^{-1})$

```
   DOUBLE PRECISION A(10,10),A1(10,10),AA1(10,10),
  1   A2(10,10),B(10),C(10),D(10,9)
10 K=1
   READ1, N,M,MD,MFLAG
 1 FORMAT(412)
   DO12 I=1,N
12 READ2,(A(I,J),J=1,N)
   DO 15 J=1,MD
15 READ2, (D(I,J),I=1,N)
 2 FORMAT(8F10.2)
   PRINT9,N,M
 9 FORMAT(3H1N=,12,3H M=,I2//)
   DO 20 I=1,N
20 PRINT3,(A(I,J),J=1,N)
 3 FORMAT(10F13.5)
   PRINT8
 8 FORMAT(1HO)
   DO 21 I=1,N
21 PRINT3, (D(I,J),J=1,MD)
   PRINT8
   DO 22 I=1,N
   DO 22J=1,N
22 A1(I,J)=A(I,J)
   CALL DPMTNV (A1,10,N)
   DO 30 I=1,N
30 PRINT4,(A1(I,J),J=1,N)
 4 FORMAT(10E13.5)
   T1=0.0
   PRINT8
   CALL DMXMLT (A,A1,AA1,N,N,N,10,10,10)
   NN=N-1
   DO 32 I=1,NN
   II=I+1
   DO 32 J=II,N
   X=AA1(I,J)
   X=ABS(X)
32 T1=T1+X
   DO 34 I=2,N
   NN=I-1
   DO 34 J=1,NN
   X=AA1(I,J)
   X=ABS(X)
34 T1=T1+X
36 DO 40 I=1,N
   PRINT4, (AA1(I,J),J=1,N)
   DO 38 J=1,N
38 AA1(I,J)=-AA1(I,J)
40 AA1(I,I)-AA1(I,I)+2.0
   CALL DMXMLT (A1,AA1,A2,N,N,N,10,10,10)
   PRINT 8
```

FIGURE 34 PROGRAM TO SOLVE AX = D USING $A_{i+1}^{-1} = A_i^{-1}(2I - AA_i^{-1})$

```
   DO50 I=1,N
50 PRINT4,(A2)I,J),J=1,N)
   PRINT8
   CALL DMXMLT (A,A2,AA1,N,N,N,10,10,10)
   T2=0.0
   NN=N-1
   DO 51 I=1,NN
   II=I+1
   DO 51 J=II,N
   X=AA1(I,J)
   X=ABS(X)
51 T2-T2+X
   DO 53 I=2,N
   NN=I-1
   DO 53 J=1,NN
   X=AA1(I,J)
   X=ABS(X)
53 T2=T2+X
   X=T1-T2
   IF(X) 55,55,70
55 PRINT5,X
 5 FORMAT(41H MATRIX ITERATION GIVES NO IMPROVEMENT X=
  1   E10.3//)
   DO 60 I=1,N
60 PRINT4,(AA1(I,J),J=1,N)
   PRINT8
   DO 65 J=1,MD
   DO 64 I=1,N
64 B(I)=D(I,J)
   CALL DMXMLT (A1,B,C,N,N,1,10,10,10)
65 PRINT4, (C(K),K=1,N)
61 IF(MFLAG)10,10,62
62 STOP
70 PRINT6,K,X,
 6 FORMAT(11H ITERATION ,12, 19H GIVES IMPROVEMENT=
  1   E10.3//)
   IF(K-M) 80,72,72
72 DO 75 J=1,MD
   DO 74 I=1,N
74 B(I)=D(I,J)
   CALL DMXMLT (A2,B,C,N,N,1,10,10,10)
75 PRINT4, (C(K),K=1,N)
   GO TO 61
80 K=K+1
   DO 85 I=1,N
   DO 85 J=1,N
85 A1(I,J)=A2(I,J)
   T1=T2
   GO TO 36
   END
```

FIGURE 34 (CONTINUED)

CHAPTER VI

SUMMARY AND CONCLUSIONS

It has been shown that the effusion of an isotopically pure gas from a closed volume through a single membrane produces a pressure waveform that is exponential in time if there is molecular flow. The time constant of this waveform can be measured to about one part in eight hundred by matching it to an electrical RC discharge. A least-square-fit method of determining time constants, which is applicable to waveforms other than simple exponentials, gives about the same accuracy. The time constants for molecular flow were found to vary directly with the square root of the molecular weight as predicted theoretically.

Temperature transients were found to be small and to dissipate in less than one second. However, even small temperature differences produced in the vacuum system by outside influences are a serious problem when making accurate pressure difference measurements because of the direct proportionality of pressure and temperature. The vacuum system must be well insulated thermally.

Because pressure waveforms can be determined with sufficient accuracy, there is the possibility of designing a vacuum system that will produce a peaked response from which the composition of gas mixtures may be determined. It has been shown how important is the choice of parameters for such a system.

The number of gases in a mixture that can be analyzed and the resulting uncertainty in the analysis are strongly dependent upon

the accuracy of the data and closeness of the molecular weights as well as the relative proportions in the mixture. Four-place data would seem to limit the number of components in an analyzable mixture to four.

Among the advantages (Kendall, 1966 and Kendall and Pulfrey, 1968) of such a gas analyzer are its inherent simplicity and ruggedness. It could work at pressures from below 10 microns to above 10 Torr with no need for an ion source, electric or magnetic fields or an ion detector. There would be little likelihood of any chemical changes in the gas mixture caused by this method of analysis.

BIBLIOGRAPHY

1. Adzumi, H., Bull. Chem. Soc. Japan, 12, 304 (1937).

2. Barnes, C. B., Vacuum, 14, 429 (1964).

3. Barrer, R. M. and D. Nicholson, Brit. J. Appl. Phys., 16, 1377 (1965).

4. Barrer, R. M. and D. Nicholson, Brit. J. Appl. Phys., 17, 1091 (1966).

5. Bodewig, E., Matrix Calculus, North-Holland (1959).

6. Buckingham, E., and J. D. Edwards, Bull. Bur. Stand., 15, 573 (1920).

7. Clausing, P., Physica, 9, 65 (1929).

8. Clausing, P., Physica, 12, 961 (1932).

9. Devienne, F. M., Rarefied Gas Dynamics, Pergamon Press (1960).

10. Dushman, S., (Ed. J. M. Lafferty) Scientific Foundations of Vacuum Technique, Wiley (1962).

11. Eden, M. et. al., Anal. Chem., 23, 1735 (1951).

12. Fryer, G. F., Proc. Roy. Soc., 293, 329 (1966).

13. Gaede, W., Ann. Phys., 41, 289 (1913).

14. Hirsch, E. H., J. Appl. Phys., 32, 977 (1961).

15. Iczkowski, R. P.,et. al., J. Phys. Chem., 67, 229 (1963).

16. Jost, W., Diffusion, Academic Press (1952).

17. Kendall, B. R. F., Proc. 14th Ann. ASTM Conf. on Mass Spec., Dallas, Texas (May 1966), p. 96.

18. Kendall, B. R. F., J. Vac. Sci. Tech., 5, 45 (1968).

19. Kendall, B. R. F. and R. E. Pulfrey, Proc. 4th Int. Vacuum Congress A.V.S., Pergamon Press (1968).

20. Kendall, B. R. F. and R. E. Pulfrey, J. Vac. Sci. Tech. (in press).

21. Kennard, E. H., Kinetic Theory of Gases, McGraw-Hill (1938).

22. Knudsen, M., Ann. Phys., 28, 75 (1909).

23. Knudsen, M., The Kinetic Theory of Gases, Methuen (1934).

24. Knudsen, M., Ann. Phys., 34, 593 (1911).

25. Lyubitov, Y. N., Molecular Flow in Vessels, Consultants Bureau (1967).

26. Nerken, A., Vac. Symp. Tran. A.V.S., Pergamon Press (1956), p. 1.

27. Oatley, C. W., Brit. J. Appl. Phys. 8, 15 (1957).

28. Patterson, G. N., Molecular Flow of Gases, Wiley (1956).

29. Pollard, W. G. and R. D. Present, Phys. Rev., 73, 762 (1948).

30. Ruthberg, S., Proc. 11th Ann. Vac. Sym. A.V.S., Paper 10-1 (1964).

31. Scott, D. S. and F. A. L. Dullien, A.I.Ch.E.J., 8, 293 (1962).

32. Scheidegger, A. E., Physics of Flow Through Porous Media, Macmillan (1960).

33. Smith, C. G. and G. Lewin, J. Vac. Sci. Tech., 3, 92 (1966).

34. Smoluchowski, M., Ann. Phys., 33, 1559 (1910).

35. Steckelmacher, W., Vacuum, 16, 561 (1966).

36. Teubner, W., Exper. Tech. Phys., 10, 278 (1962).

37. Weber, S., Mat. Fys. Medd., 28, No. 2 (1954).

38. Wheeler, A., Advan. Catalysis, 3, 250 (1951).